COMPUTATIONAL VIEW OF SURFACE BASED ORGANIC MASS SPECTROMETRY

Barbara J. Garrison[1]* and Zbigniew Postawa[2]*
[1]*Department of Chemistry, Penn State University, 104 Chemistry Building, University Park, Pennsylvania 16802*
[2]*Jagellonian University, Smoluchowski Institute of Physics, ul. Reymonta 4, 30-059 Kraków, Poland*

Received 21 September 2007; received (revised) 10 December 2007; accepted 18 December 2007

Published online 17 April 2008 in Wiley InterScience (www.interscience.wiley.com) DOI 10.1002/mas.20165

Surface based mass spectrometric approaches fill an important niche in the mass analysis portfolio of tools. The particular niche depends on both the underlying physics and chemistry of molecule ejection as well as experimental characteristics. In this article, we use molecular dynamics computer simulations to elucidate the fundamental processes giving rise to ejection of organic molecules in atomic and cluster secondary ion mass spectrometry (SIMS), massive cluster impact (MCI) mass spectrometry, and matrix-assisted laser desorption ionization (MALDI) mass spectrometry. This review is aimed at graduate students and experimental researchers. © 2008 Wiley Periodicals, Inc., Mass Spec Rev 27:289–315, 2008

Keywords: *computer simulation; molecular dynamics; atomic SIMS; cluster SIMS; MALDI*

I. INTRODUCTION

Surface based mass spectrometry in which an energetic probe (atomic ion, cluster ion, or laser) strikes a surface and non-volatile molecules are emitted for analysis are counter intuitive as to their efficacy. In secondary ion mass spectrometry (SIMS), an atomic ion with tens of keV of incident energy strikes a surface ejecting molecules with masses up to tens of kDa. The incorporation of small clusters such as SF_5^+, Au_3^+, Bi_3^+, and C_{60}^+ as incident ion sources for SIMS experiments has in many instances increased the total yield of ejected particles and the ion fraction, therefore opening the door for molecular depth profiling experiments (Winograd, 2005). An increase of the cluster size to thousands of atoms is expected to shift the detection to higher masses. Further increases of cluster size up to micron sized droplets with a total of GeV of energy introduces the mass spectrometric approaches of massive cluster impact (MCI) (Mahoney et al., 1992; Cornett, Lee, & Mahoney, 1994; Tempez et al., 2004; Li, Verkhoturov, & Schweikert, 2006), electrospray droplet impact (EDI) (Hiraoka et al., 2006a; Hiraoka, Mori, & Asakawa, 2006; Asakawa et al., 2007) and desorption electrospray surface ionization (DESI) (Takats et al., 2004; Takats, Wiseman, & Cooks, 2005; Cooks et al., 2006). The intrigue with the approaches such as DESI is that the experiments are performed under atmospheric conditions without the need for ultrahigh vacuum equipment. Finally, the use of pulsed lasers as the probe as in matrix assisted laser desorption ionization (MALDI) is a mainstay in mass spectrometry of large biomolecules (Hillenkamp et al., 1991).

The process by which an energetic probe with total energy many times greater than the bond strength of the individual molecules in the sample vaporizes a non-volatile molecule intact is not obvious. In this article, we use results from molecular dynamics (MD) computer simulations to illustrate the basic processes in each technique, and to elucidate how the basic physics influences what is measured. In particular, we focus on the amount of cooperation in the atomic and molecular motions that give rise to the ejection event which is a key feature to the nature of the measured quantities including the size of the ejected molecules. We will consider model systems as shown in Figure 1. The first three systems are for simulations of atom and cluster bombardment of solids. The first (Fig. 1a) and third (Fig. 1c) systems consist of thin layers of molecules such as benzene, polystyrene (PS) oligomers or water on a metal substrate. Different sized systems are used depending on the amount of motion generated in the substrate. The second system (Fig. 1b) is a molecular solid of benzene represented by a coarse-grained description. For all the simulations using this system, the kinetic energy of the incident particle has been limited to 5 keV of incident energy because the sample would have to be larger for increased kinetic energy which would challenge the computational feasibility. Finally, for the MALDI simulations, the solid consists of analyte molecules embedded in a matrix (Fig. 1d). It should be noted that for the cluster bombardment studies, all the action occurs in the middle of the sample. As discussed in the MALDI section, for the MALDI simulations, the entire system represents only the center of the laser beam because the size of the laser spot is too large to model effects at the edge of the laser spot. The differences in size scale are intertwined with the important physics involved in each process. We first give an overview of the MD approach and then discuss atomic SIMS, cluster SIMS, MCI, and then MALDI.

This article contains supplementary material, which may be viewed at the Mass Spectrometry Reviews website at http://www.interscience.wiley.com/jpages/0277-7037/suppmat/mas.20165.html.

Contract grant sponsor: National Science Foundation; Contract grant number: CHE-0456514; Contract grant sponsor: Polish Ministry of Science and Higher Education; Contract grant numbers: PB 4097/H03/2007/33, PB2030/H03/2006/31.

**Correspondence to:* Barbara J. Garrison,
E-mail: bjg@psu.edu and Zbigniew Postawa,
E-mail: zp@castor.if.uj.edu.pl

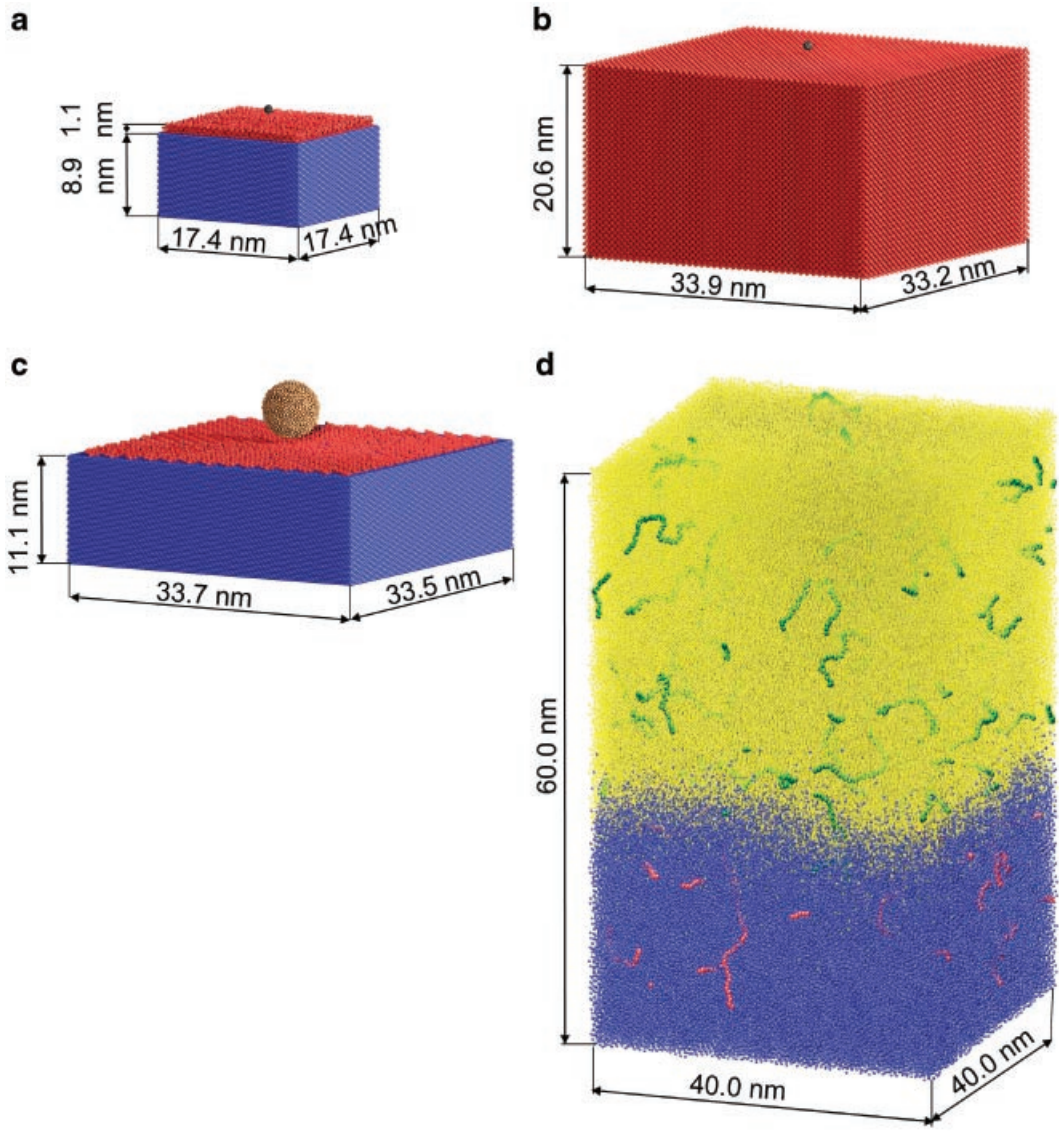

FIGURE 1. Systems used in the simulations. **a**: Three layers of benzene molecules (red) adsorbed on a Ag substrate (blue). Projectiles (black) including atomic particles and C_{60}. The organic molecules (benzene) are described with the atomistic AIREBO potential. **b**: Solid of benzene molecules (red) modeled with a coarse-grained interaction potential. **c**: Monolayer of polystyrene tetramer (PS4) (red) adsorbed on a Ag substrate (blue). The projectile (peach) is Ar_{9000}. **d**: System used in the MALDI simulations. The penetration depth is 50 nm. Matrix and analyte molecules that eject are colored yellow and green, respectively. Matrix and analyte molecules that do not eject are colored blue and red, respectively. Periodic boundary conditions are applied in the horizontal directions and there is a pressure absorbing boundary condition at the bottom of the sample.

II. MOLECULAR DYNAMICS TECHNIQUE

The emphasis in this section is on describing the essential elements of molecular dynamics (MD) simulations that we feel are important for a non-expert to understand and appreciate the results of the simulations. Recipes for actually performing simulations are published elsewhere (Allen & Tildesley, 1987; Frenkel & Smit, 2002). Previous articles describing the application of MD simulations to SIMS (Garrison, 1992, 2001) are available, as well as articles describing the strategies for performing MALDI or laser ablation simulations (Zhigilei, Kodali, & Garrison, 1998; Zhigilei et al., 2003a).

The classical equations of motion are implemented in the form of first order differential equations for the time development of the velocity and position of the particles as

$$m_i \frac{\mathrm{d}\mathbf{v}_i}{\mathrm{d}t} = \mathbf{F}_i = -\mathrm{grad}\, V(\mathbf{r}_1, \mathbf{r}_2, \ldots \mathbf{r}_{\mathrm{Natoms}}) \qquad (1a)$$

$$\frac{d\mathbf{r}_i}{dt} = \mathbf{v}_i \tag{1b}$$

where m_i, $\mathbf{r}_i$, $\mathbf{v}_i$, $\mathbf{a}_i$, and $\mathbf{F}_i$ are the mass, position, velocity, acceleration and force of the ith particle. The simplest conceptual representation of a particle is to consider it to be an atom and there are a total of N_{atoms} in the system. Below we discuss grouping several atoms together into one particle in the simulation. The interaction potential, $V(\mathbf{r}_1, \mathbf{r}_2, \ldots \mathbf{r}_{Natoms})$, is generally a function of the positions of all the particles. The position, velocity, acceleration and force are all vectors in three dimensions. The solution to the differential equations is performed numerically for a time step δt.

A. Assumptions of Classical Mechanics

The equations of motion are classical in nature. No quantum effects of any kind are included and no excited electronic or ionic states are taken into account. Thus, ionization is beyond the scope of classical mechanics. The particles are considered to be in their lowest electronic state during the entire simulation. There is no coupling or transfer of energy between the electronic and nuclear degrees of freedom. These assumptions are, of course, not 100% valid. Properties that we feel should be well described by classical mechanics include the general region of the target where the energy is deposited, general ejection mechanisms, crater formation, and substrate mixing. These motions must occur regardless of whether the species are neutral or ionic. The biggest challenge of the MD simulations in terms of accurately modeling the surface based mass spectrometry is the lack of incorporation of ionization mechanisms. Virtually all surface based mass spectrometric techniques detect ions that are formed naturally during the ejection process. The calculations predict information about the ejected neutral species. Thus direct comparisons of mass spectra, kinetic energy distributions, and angular distributions between the experimental data and the calculated results must be treated with caution. Ultimately, the test of the results of classical dynamics simulations is the utility in explaining experimental results. We hope the insights presented in this article illustrate that the simulations are useful.

B. Force or Interaction Potential

The essential ingredient in Eq. (1a) for describing realistically atomic motions, especially in the chemical regime, is the nature of the force or interaction potential. In general physical chemistry terms, the interaction potential is the solution to the electronic Schrödinger equation within the Born-Oppenheimer approximation (Atkins & dePaula, 2006). In principle, one could solve the Schrödinger equation for each configuration of atoms shown in the figures in this article and evaluate the forces. Computer speeds are not yet sufficient, however, to consider a direct evaluation of the Schrödinger equation during the simulations with thousands to millions of particles. Thus, the approach most commonly employed is to use a mathematical formula with a functional form that can represent the actual solution of the Schrödinger equation. The parameters of the functional form are fit to available experimental data. The challenge is to obtain sufficient experimental data and to have a functional form that reasonably represents the chemistry and physics of the system. The empirical potentials are often used for configurations that are far from the configurations for which they are fit. Care must always be taken that the results from the simulations are sensible and comparison with experimental data is an on-going critical component of the modeling venture.

During the 1980s, efforts were made by several groups to develop empirical potentials for reactions that include many-body effects, that is, the interaction between a pair of atoms changes depending on other atoms nearby (Garrison & Srivastava, 1995). The most developed potentials are those for face centered cubic metals and group IV (silicon, germanium, and carbon) elements. Examples of popular potentials for fcc metals include the Sandia embedded atom method (EAM) (Foiles, Baskes, & Daw, 1986) and the molecular dynamics-Monte Carlo corrected effective medium MD/MC-CEM (Kelchner et al., 1994) potentials. For Si, popular potentials have been developed by Stillinger and Weber (1985) and Tersoff (1988, 1989). One potential of recent interest to the SIMS community was developed by Brenner for reactions of hydrocarbon molecules (Brenner, 1990; Brenner et al., 2002). In this potential, the bond strength changes depending on the coordination number, bond angles and conjugation effects, and therefore, the potential is able to model bond breaking and bond formation. Brenner conceived a sufficiently flexible functional form that he could fit it to the plethora of experimental data available for bulk phases of carbon as well as small hydrocarbon molecules. His initial interest was modeling diamond film growth but other researchers have used the potential for a variety of processes in which reactions occur (Garrison, Kodali, & Srivastava, 1996). Stuart, Tutein, and Harrison (2000) have incorporated a long-range interaction term to the Brenner potential in a manner so that there are interactions among non-bonded species. Their AIREBO potential is used in several of the simulations described below.

The utopia of having a perfect interaction potential for a system may be an impossible dream. Many of the basic processes that we are modeling, however, are general to a wide range of systems. For example, the angular distributions of ejected atoms from the (100) face of face-centered-cubic surfaces are very similar and strongly reflect the surface arrangement rather than the specifics of a particular metal. There are several molecules that work well as MALDI matrices. We believe that the simulations model the basic ejection process of MALDI but issues such as compatibility of one matrix with a specific analyte and ionization are beyond the scope of the present simulations. It is important, therefore, to know what properties of the model system are comparable to the real system and not to over interpret results from the simulations. This knowledge comes to a large extent with experience and with continual interplay with experimental researchers and their results.

C. Alternative Choices for a Particle

The traditional choice of particle in the MD simulations is an atom but as discussed below the amount of computer time needed to model processes with hundreds of thousands of atoms using sophisticated and computationally intricate potentials like

AIREBO becomes prohibitive. Thus, groups of atoms are coarse-grained (CG) and represented as one united particle or atom. For the simulations presented here, two choices have been implemented. For the molecular solid comprised of benzene, the C and H atom are coarse-grained into one CH particle (Smiley et al., 2006; Smiley, Winograd, & Garrison, 2007). For the simulations of MALDI or laser ablation, the entire matrix molecule is coarse-grained into one particle (Zhigilei, Kodali, & Garrison, 1997; Zhigilei et al., 1998, 2003a). Not only are there fewer particles, but in general, the interaction potentials are much simpler and less costly to evaluate. The downside of the simpler united atom representation is the inability to consider broad based chemical reactions as is possible with the AIREBO potential. Limited chemical reactions such as C–C bond cleavage are incorporated for benzene molecules in SIMS simulations and analyte molecules in MALDI. This limited ability to consider bond breaks does allow us in the simulations to monitor if the conditions are right for chemical reactions to occur. A more complex approach for considering wide-spread chemical reactions in laser ablation studies has been developed (Yingling, Conforti, & Garrison, 2004; Prasad, Conforti, & Garrison, 2007) but will not be discussed here.

D. Numerical Integration and Time Step

Solving the equations of motion, Eq. (1), involves numerical integration. The challenge to solving Eq. (1) is that the force, **F**, (or interaction potential) is a function of all the positions of all the particles. The positions depend on the time. The standard approach in numerical integration is to choose a time step, δt, during which $\mathbf{F}/m$ and $\mathbf{v}$ are approximately constant. An overly simplistic yet illustrative solution to Eq. (1) is then

$$\mathbf{v}_i(t+\delta t) = \frac{\mathbf{v}_i(t) + \mathbf{F}_i(\mathbf{r}(t))}{m_i}\delta t \tag{2a}$$

$$\mathbf{r}_i(t+\delta t) = \mathbf{r}_i(t) + \mathbf{v}_i(t)\delta t \tag{2b}$$

The evolution of all the positions and velocities during the trajectory thus occurs in discrete steps. Knowledge of the velocities allows one to calculate quantities such as angles of motion, kinetic energy, temperature, and pressure. The positions as a function of time yield a microscopic picture of the motions as shown in several figures and animations in this article. The positions and velocities combined together give information about molecules and clusters. The integrator in Eq. (2) is only for illustration and is vastly oversimplified. Appropriate algorithms can be found in simulation texts along with formulae for calculating distributions, temperature and pressure (Allen & Tildesley, 1987; Frenkel & Smit, 2002).

The criterion for an acceptable time step is whether energy is conserved as a function of time during the course of the numerical integration. This computational check is a very convenient aid in choosing the time step. Given that energy must be conserved, what is considered a large and small time step? We typically run our simulations of the SIMS process with an integrator that allows us to vary automatically the time step during the collision cascade. Otherwise, we would have to use the smallest time step necessary for integration of the entire trajectory. The time steps vary from as small as 0.01 fsec (femtosecond or 10^{-15} sec) at the beginning of the simulation to nearly 1 fsec at the end of the simulation. The conditions of MALDI of uniform motion during the course of the simulation are such that a fixed time step, typically around 5 fsec, is used for the whole simulation (Zhigilei et al., 1997, 1998).

E. Initial Conditions

To initiate the integration of the equations of motion, Eq. (1), the positions and velocities at time $t = 0$ must be prescribed for all particles. For this discussion, we consider the SIMS simulations. The novel features of incorporating the laser beam are discussed in the section on MALDI. First, we will examine the initial conditions of the incident particle and then the substrate particles.

1. Incident Particle

The initial velocity vector is chosen from the experimental energy and angle of incidence. The initial height above the surface of the incident particle is chosen so that there is no interaction with the surface. In principle, this value should be infinity but because the interaction potential or force is truncated at some distance, the starting height is typically 1–2 nm above the surface. Finally, the incident particle must be aimed at a specific lateral position on the surface. For atomic bombardment the dynamics of the collision cascade can be very different if the incident particle makes a head-on collision with one atom or enters a channel. As a result, one must calculate the motion in the solid for many different aiming points that represent all possible positions on the surface. Fifteen aiming points for 15 keV Ga bombardment on a system of three layers of benzene on an Ag substrate are shown in Figure 2a. The molecular yield for each aiming point is given in Figure 2b, left panel. The yields range from 15 to 454 with an average value of 229 ± 32 benzene molecules. For C_{60} bombardment, the molecular yield for each aiming point is shown in Figure 2b, right panel, and has an average value of 382 ± 4. The amount of diversity of action influences how many incident aiming points must be sampled in performing the simulations. As a result, hundreds of impact points are required for atomic projectiles while just a few impacts are usually sufficient for large clusters (Postawa et al., 2003). Each aiming point of the primary particle and subsequent motion is called a trajectory.

2. Sample

The initial positions of the particles in the system are chosen to best match the experimental ones. For ordered systems (single crystals, ordered overlayers), the assignment of positions is relatively straightforward. If one, however, wants to model a disordered system, there are challenges. For example, if the experimental sample is a polycrystalline metal, can one really define the distribution of crystalline surfaces, the orientation of the crystallites at the surface, the size of the individual crystallites, etc? There is no universal answer. One needs to use judgment and experience to figure out if a model system can be used to give insight into the experimental data. The initial

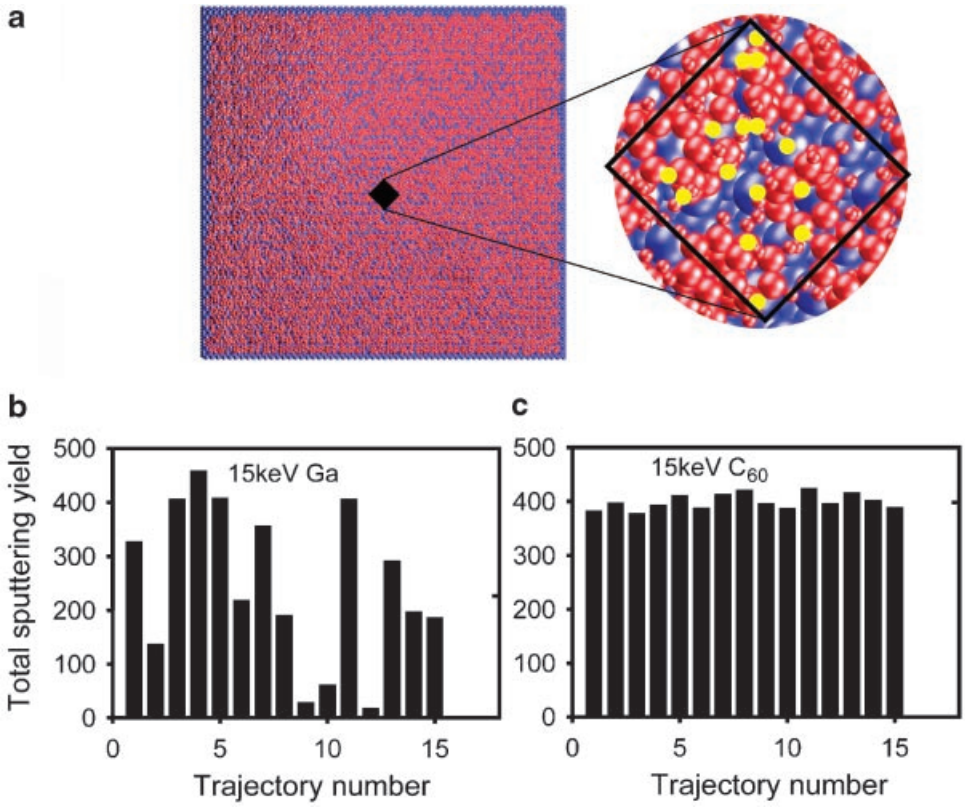

FIGURE 2. Diversity of action for various aiming points for three layers of benzene on Ag. **a**: Fifteen different aiming points (yellow). **b**: Sputtering yield in benzene molecule equivalents vs individual aiming points for 15 keV Ga bombardment. The average is 229 ± 32. **c**: Sputtering yield in benzene molecule equivalents versus individual aiming points for 15 keV C_{60} bombardment. The average is 382 ± 4. The dashed line indicates the average yield.

velocities are often assumed to be zero although they can be selected to satisfy a desired thermal distribution. The objective is always to incorporate the experimentally relevant distributions of positions and velocities as best as it is possible to do.

F. Final Conditions

The numerical integration for one aiming point of the primary particle or one laser fluence is terminated when the number of ejected particles remains constant. Once the trajectory is finished, one then examines pictorially and/or mathematically the final positions and velocities. The average yield of particles ejected can be determined by counting the particles above the surface and dividing by the number of aiming points selected for the incident projectiles. Calculating the kinetic energy distribution of the ejected material is a straightforward process using $\frac{1}{2}m_i v_i^2$ for each particle. Likewise, the velocity vectors can be used to determine an angular distribution. The final positions and velocities are used to determine whether clusters and molecules are ejected. For MALDI, the ablation process can be driven by temperature and/or pressure, quantities that can be determined in the simulation from velocities and positions.

Information about molecules and clusters is the tricky item to calculate. The simulations are typically run for 1–30 psec whereas the flight time to the detector is on the order of 10 μsec. Molecules and clusters that are internally excited can decay on the flight to the detector. For metal clusters, the fate of the ejected clusters can be determined by following their motion for longer times (Wucher & Garrison, 1992) because the interaction potential is reasonable for the dissociation processes, and the time scale of dissociation is tens of picoseconds. The calculations show that the dissociation processes must be included in order to obtain the correct energy and angular distributions (Wucher & Garrison, 1992). For hydrocarbon molecules such as those described by the AIREBO potential there are two challenges for performing similar simulations. First, the time scale of dissociation and rearrangement can be longer than flight time to the detector and simulations of a microsecond time scale are not tractable. Second, it is not clear that the interaction potential accurately represents all the possible rearrangement channels. Thus, the strategy has been to use a statistical model to estimate the amount of internal energy below which the molecule will remain intact to reach the detector (Delcorte & Garrison, 2000). Molecules with more than this amount of energy are considered fragmented but no assumption is made about the fragmentation channels and thus no correction can be made to the energy and angular distributions of the fragment species. The most challenging molecular type is cluster of molecules, for example $(C_6H_6)_n$. Classical mechanics allows

energy flow between the high-frequency intramoleculer vibrational modes with the low frequency intermoleculer motion, phenomenon not allowed quantum mechanically. Generally details about such clusters are ignored (Postawa et al., 2005).

Finally, the particle motions giving rise to any particular event or sets of events can be extracted to understand why a certain event occurs. It is the correlation of the microscopic basis of particle motions with experimental data that is the real strength of the MD simulations to understand surface based mass spectrometry.

G. Computer Time

The total computer time depends on several factors including time step in the integration, total length of the motion, the number of trajectories that need to be sampled and the length of the force calculation. The range of time steps varies from 0.01 to ~1 femtoseconds. The total length of time of a trajectory can vary from a hundred femtoseconds for atomic SIMS of metal substrates to tens of picoseconds for cluster SIMS to almost a nanosecond for MALDI. The number of trajectories needed varies depending on the cluster size and the final quantities being calculated. For quantities such as total yield of particles emitted in atomic SIMS calculations, typically 100–500 different aiming points are sufficient. On the other hand, for high resolution energy and angle resolved distributions 500–3,000 aiming points are required. For cluster bombardment and laser irradiation one trajectory is typically sufficient to estimate the yield and between 10 and 20 trajectories should be sampled for kinetic energy and angular distributions for a given set of initial conditions because the statistical deviation as shown in Figure 2b is small.

The evaluation of the force is the most time consuming part of each integration step. The computer time of the force calculation depends on several factors including the number of particles, the number of neighbor particles that interact with the particle and the complexity of the force evaluation. For example, the AIREBO potential (Stuart et al., 2000) is very long ranged with as many as 300 neighbor atoms of each atom and is very computationally expensive to evaluate.

In Table I are computer times along with the system sizes for the animations given in this article. The times vary from a day to a couple of months. The use of the computationally intensive AIREBO potential is in general limited to hydrocarbon overlayers on a metal substrate. Even the coarse-grained benzene system is only used for 5 keV bombardment and not higher, more experimentally relevant energies like 20 keV. The MALDI (i.e., laser ablation) simulation which has one particle per matrix molecule allows for the largest system size.

III. ATOMIC SIMS

The essential motion associated with atomic SIMS involves an ion such as Ar^+, Ga^+, O^+, or Cs^+ with several eV of kinetic energy bombarding a sample. Over the years, an extensive number of MD simulations have been performed aimed at understanding various aspects of the physics and chemistry of the process and many comparisons have been made to experimental

TABLE I. Typical computer times for one trajectory on different systems

System	Number of particles	Volume (nm^3)	Time of Trajectory	Computer Time
15 keV Ga bombarding 3 layers of AIREBO benzene on Ag	14904 C and 14904 H atoms; 166530 Ag atoms	$2.9x10^3$	26 ps	5 days
5 keV Au bombarding molecular solid of CG benzene	1192320 CH particles	$2.4x10^4$	36 ps	1 month
15 keV C_{60} bombarding 3 layers od AIREBO benzene on Ag	14904 C and 14904 H atoms; 166530 Ag atoms	$2.9x10^3$	26 ps	6 days
20 keV C_{60} bombarding a PS61 molecule deposited on Ag	491C and 499 H atoms; 166530 Ag atoms	$2.8x10^3$	9 ps	1 day
18 keV Ar_{9000} PS4 monolayer deposited on Ag	16128 C and 18816 H atoms; 611442 Ag atoms	$1.0x10^4$	36 ps	12 days
8.72 keV Ar_{872} bombarding molecular solid of CG benzene	1192320 CH particles	$2.4x10^4$	36 ps	2 months
MALDI Animation	669192 molecules/units	$9.6x10^4$	1200 ps	1.5 months

The first six simulations were run in serial on the lion-xo cluster (http://gears.aset.psu.edu/hpc/systems/lionxo/) consisting of Dual 2.4 GHz AMD Opteron Processors. The MALDI simulation was run on a similar machine.

data (Garrison, 2001). The physics of the atomic motions can be conceptualized as a sophisticated game of billiards in which each atom is a particle. The forces or interactions among the atoms are described by the chemistry of the system.

There are many aspects of atomic SIMS that make it an ideal case for examination by MD simulations. The total time for particles to eject from systems with moderate binding energies, that is, not van der Waals solids, is less than a few picoseconds, a tractable time for MD simulations. The ejected (or sputtered) particles tend to come from the near surface region, thus the number of particles needed in the simulation can be on the order of several thousand, again a tractable number. As discussed above, the motion from many aiming points are averaged in order to compare with experimental data. We start first with simulations of thin organic layers on a metal substrate and then discuss a molecular solid.

A. Thin Organic Layer

The ejection of molecules from a metal surface due to atomic bombardment has been studied by our group for over two decades. An example of a collision cascade from one trajectory is shown in Figure 3 and *Animation 1*. In this case, the incident particle is a Ga atom with 15 keV of kinetic energy. The sample consists of three layers of benzene on a Ag(111) substrate (Postawa et al., 2005). The interactions among the atoms in the benzene molecules are described by the atomistic AIREBO potential (Stuart et al., 2000). Figure 3a shows the atomic positions at three times and Figure 3b gives the atomic displacements at the same three times for a trajectory that gives approximately the average yield. The atomic displacements give several hints as to the important processes taking place. First, as shown by the red arrow, the Ga projectile implants ~3.7 nm deep into the sample. This depth is typical of ranges of ions in metal substrates as determined by SRIM calculations (Ziegler, Biersack, & Littmark, 1985). The atomic projectile is thus depositing the initial energy over a fairly long distance. Consistent with this observation, we see that Ag particles along the path of motion of the Ga projectiles have been displaced. Atomic mixing both in the lateral and vertical directions is a well known effect of energetic bombardment of atomic solids (Ziegler et al., 1985). The particles that are displaced the most (red) are the surface benzene molecules. As discussed below, the energy deposited in the metal substrate is the main source of the motion that gives rise to the molecular ejection.

The diversity of action is shown in Figure 2 for the same three layers of benzene on Ag system. Figure 2a denotes fifteen different aiming points on the surface and Figure 2b gives the molecular yield from each trajectory. The aiming point in which there is very low ejection yield involves the incident particle penetrating deep in the sample and depositing its energy away from the surface region. Aiming points that give rise to the largest ejection yields involve motions in which the primary particle deposits a large amount of energy in the top couple of metal layers (Delcorte, 2000). The large number of aiming points (projectile ions in the experiment) that give very little useful signal has been one of the frustrations in atomic SIMS and one of the reasons for pursuing cluster SIMS as discussed below.

The substrate plays a major role in sputtering of thin organic overlayers. Almost all intact molecules are ejected by collective motion (Garrison, 1980; Chatterjee et al., 1999; Garrison, Delcorte, & Krantzman, 2000). An example of this type of motion is shown in Figure 4 for a polystyrene tetramer, PS4, ejecting from a silver substrate. There is one PS4 molecule shown. At the time of the snapshot, several Ag atoms are above the original surface and are moving upward 'together' pushing the molecule upward towards the vacuum (and ultimately the detector) without being in thermal equilibrium with the internal vibrational modes. This concerted motion of several substrate atoms pushing upward on molecule occurs when the incident hits the surface 'just right.' The ejection of intact molecules in atomic SIMS is thus an occasional event, that is, the physics of the emission process does not demand that every ion hit create upward motion near the surface. As discussed below, other probes do demand that there be concerted upward motion for every energy deposition event. For example, in MALDI, the ablation dynamics is a phase explosion that occurs for every laser pulse that pushes massive amounts of material towards the vacuum. We believe that the lack of collective upward motion in the collision cascades is the reason that the largest mass (tens of kDa) observed in atomic SIMS is considerably less than, for example, MALDI where the largest mass is hundreds of kDa.

B. Organic Solid

Bombardment of a molecular solid by an atomic projectile as shown in Figure 5 and Animation 2 has only recently become tractable. In this simulation, the coarse-grained description of benzene was implemented and the kinetic energy of the Au projectile was limited to 5 keV. For this simulation, we used a sample size of 1.2 million particles. Only one incident trajectory was run, thus we have no information about the diversity of action for various aiming points. In the comparison of Figures 3 and 5, it is important to realize the difference in scale. In Figure 3, the sample is 17 nm wide and 11 nm deep and could contain the action of a 15 keV Ga particle. In Figure 5, the sample is 34 nm wide and 21 nm deep and the incident Au particle only had 5 keV of incident energy. The metal substrate is much more effective at containing the energy of the incident particle close to the surface because the metal atoms are more massive than the C atoms in C_{60} and the metal substrate has a higher cohesive energy than benzene. The result of the atomic projectile hitting the benzene target is a crater at 36 psec. We anticipate that this crater will fill in at a later time.

Although damage to the molecules is not explicitly shown, Figure 5b shows that there are displacements of particles to a depth of 15 nm. Moreover, the width of the altered region is 12–15 nm. It is not surprising, therefore, that it is not possible to depth profile through molecular solids with atomic projectiles. The first impact at a point on a surface creates damage over a large volume. As a result, the second impact at the same area would find mostly fragments and modified material for analysis. As we will discuss below, the damage conditions for cluster bombardment are very different.

We have chosen to discuss two main aspects of the atomic SIMS process that are consequences of the atomic motions. First,

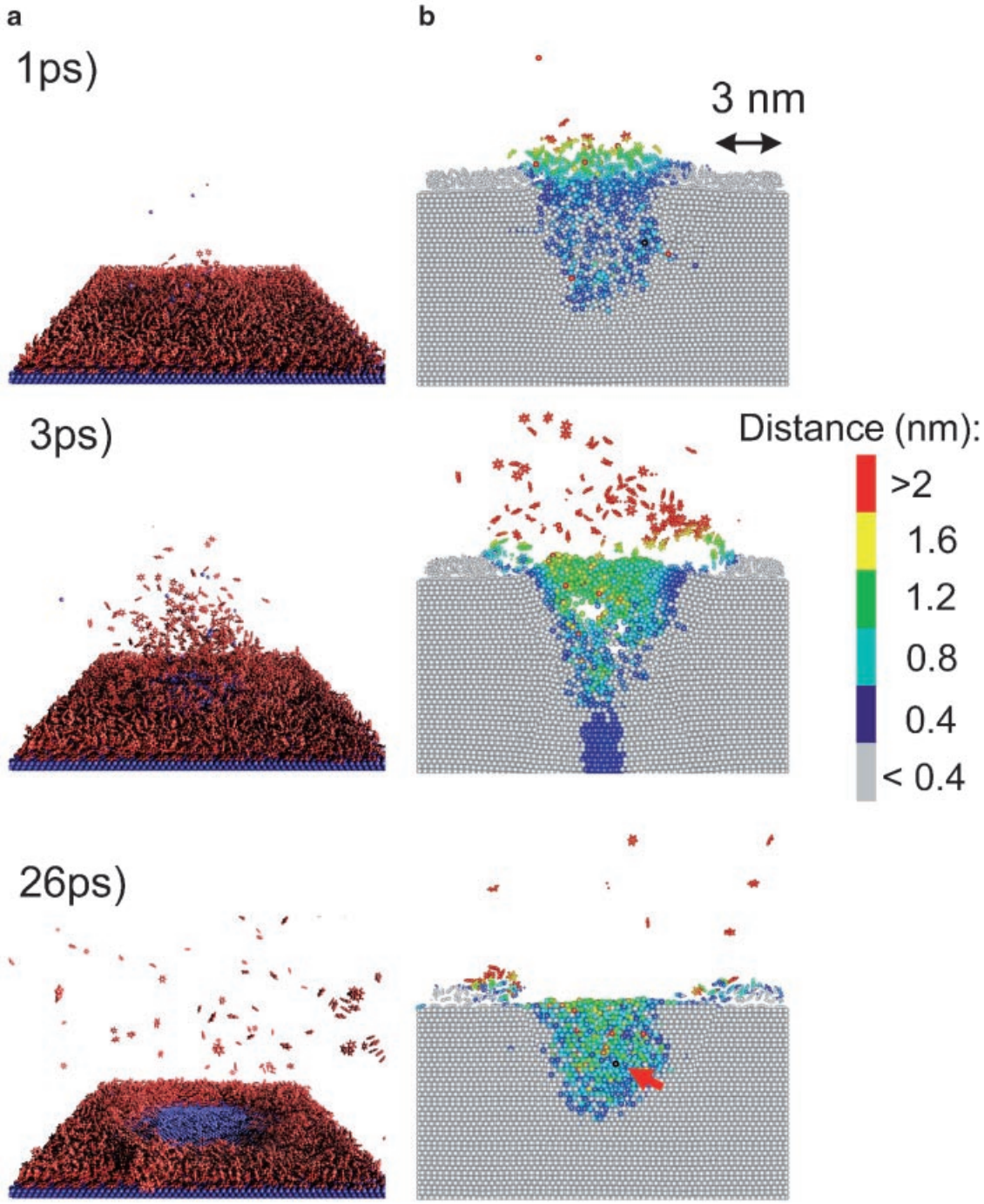

FIGURE 3. Snapshots for 15 keV Ga bombardment of three layers of benzene on Ag. **a**: Atomic positions at three times. The coloring scheme is the same as Figure 1a. **b**: A 1.5 nm slice through the center of the sample directly below the impact point. The coloring is by the amount of displacement from the initial position colored according to the legend on the right side. The red arrow depicts the final position of the incident Ga particle. *Animation 1*.

the diversity of action from one ion hit to the next means that ejection of molecules is not consistent in quantity or specific mechanism from one impact to the next. Specifically, although there is a basic similar mechanism in how molecules are ejected, the dynamics of energy dissipation does not demand that the action for ejection occurs on every ion impact. This lack of concerted motion limits the ultimate size of molecules that are ejected. Second, the long range of the incident particle into the sample creates subsurface mixing and damage to molecules in a large volume.

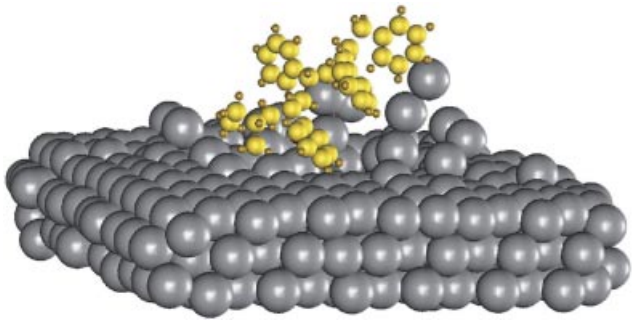

FIGURE 4. Cooperative uplifting mechanism for a polystyrene tetramer on Ag. The Ag atoms are represented by silver spheres and the C and H atoms by large and small gold spheres. Many atoms, including other PS tetramers, are omitted for visual clarity. Used by permission from the American Chemical Society, Garrison, Delcorte, and Krantzman (2000). [Color figure can be viewed in the online issue, which is available at www.interscience.wiley.com.]

IV. CLUSTER SIMS

Experimentally it has been found that in many cases the cluster beams enhance the total yield of ejected material as well as enhance the ion fraction (Weibel et al., 2003). The new cluster ion guns can be focused, maintain the ability to do 2D imaging, and have opened the door for molecular depth profiling (Winograd, 2005).

The dynamics of cluster bombardment of atomic solids shows that a crater is formed (Aoki et al., 1998; Seki et al., 1998; Webb et al., 1999; Aderjan & Urbassek, 2000; Colla et al., 2000; Colla & Urbassek, 2000; Kerford & Webb, 2001; Postawa et al., 2003; Postawa et al., 2004; Postawa et al., 2005), much like a meteor hitting the earth. For example, the diameter of C_{60} is 0.7 nm, thus it has a larger dimension than typical bond lengths in organic molecules, 0.1 to 0.2 nm, and the interatomic spacing in metals, for example, 0.29 nm in Ag. Since the motion of the atoms in the C_{60} projectile have highly correlated positions and velocities, the C_{60} initially acts as a single particle when hitting the substrate (Garrison et al., 2007). This single particle motion initially creates a crater in the substrate. The dynamics associated with the crater formation deposits the energy in the near surface region, thus enhancing the yield. Moreover, it can also restrict the damage to molecules to the near surface region. The MD simulations present a view that cluster bombardment of solids is distinctly different relative to atomic bombardment.

As with atomic bombardment, we divide our discussion into thin films on metal substrates and solid organic substrates. Our primary focus in modeling studies has been the C_{60} cluster so most of our discussion highlights those simulations. We will discuss briefly a comparison of C_{60} and Au_3 bombardment of water ice to illustrate the differences between two clusters with similar total masses but very different number of atoms and masses of individual atoms. The water studies allow us to address the issue of reaction zones in the substrate.

A. Thin Organic Layer

The physics of the bombardment event for C_{60} bombardment of three layers of benzene molecules on Ag is illustrated in Figure 6 and *Animation 3*. The trajectories chosen for illustration in Figures 3 and 6 have an average number of ejected particles as shown in Figure 2. A comparison of atomic (Fig. 3a) and cluster (Fig. 6a) bombardment of thin organic layers on metal substrates indicates that both projectiles remove molecules from about the same area on the surface (Postawa et al., 2005; Czerwinski et al., 2006; Szakal et al., 2006). Consequently, for thin films on metal substrates, there is not a large enhancement effect in ejection yield due to cluster bombardment (Weibel et al., 2003; Sostarecz et al., 2004; Winograd, 2005).

The mechanism of molecular ejection for a single monolayer arises primarily from a concerted motion associated with the crater creation as shown in Figure 7 and *Animation 4*. An impact of C_{60} at a 3 nm distance from a polystyrene (PS) 61-imer with a total mass 6.4 kDa is depicted. The crater rim formation pushes off the molecule. If the molecule is too close to the impact point, then, of course, it is broken up. If it is too far from the impact point, then it cannot eject. One might suspect because there is collective motion of many substrate atoms giving rise to molecule ejection that larger molecules might eject in cluster SIMS than atomic SIMS. To our knowledge, however, this observation has not been seen in experiment.

Increasing the thickness of the film from a single monolayer introduces additional energy transfer processes. Direct collisions between the incoming projectile and the organic molecules almost always lead to the formation of energetic fragments. These fragments can lead to more fragmentation in the overlayer, penetrate into the bulk or eject. However, during layer penetration the fragments are slowing down and finally collisions between slowed-down fragments and the organic particles can also stimulate ejection of intact molecules. The importance of this emission channel increases with the thickness of the organic overlayer and with the size of the projectile. For atomic bombardment and the overlayers much thinner than a projectile range the process is not very significant, however, it is important for cluster projectiles and coatings thicker than a monolayer.

The exciting difference arises in where the energy is deposited and the displacements in the solid, that is, compare Figure 3b with Figure 6b. The energy from the C_{60} bombardment is deposited near the surface and the displacements are confined to the crater edge. The depth of the displacements (damage) due to cluster bombardment is shallower relative to atomic bombardment. These observations have implications for molecular depth profiling as discussed in Section IV.F.

B. Organic Solid

The motion associated with C_{60} bombardment at 5 keV of a coarse-grained benzene solid is shown in Figure 8 and *Animation 5*. We will first compare C_{60} bombardment on a thin layer (Fig. 6) with the molecular solid (Fig. 8). Due to a larger binding energy, atomic density, and mass of the individual atoms composing the substrate, the metal substrate more effectively stops the C_{60} and confines the energy closer to the surface (Anders & Urbassek, 2005a, Anders et al., 2007). This conclusion is valid even with an incident energy of 15 keV for the thin layer system versus 5 keV for the molecular solid. The metal does play an important role absorbing the energy of the cluster and in the ejection of the organic molecules. In the case of the benzene solid, the projectile goes deeper in the sample.

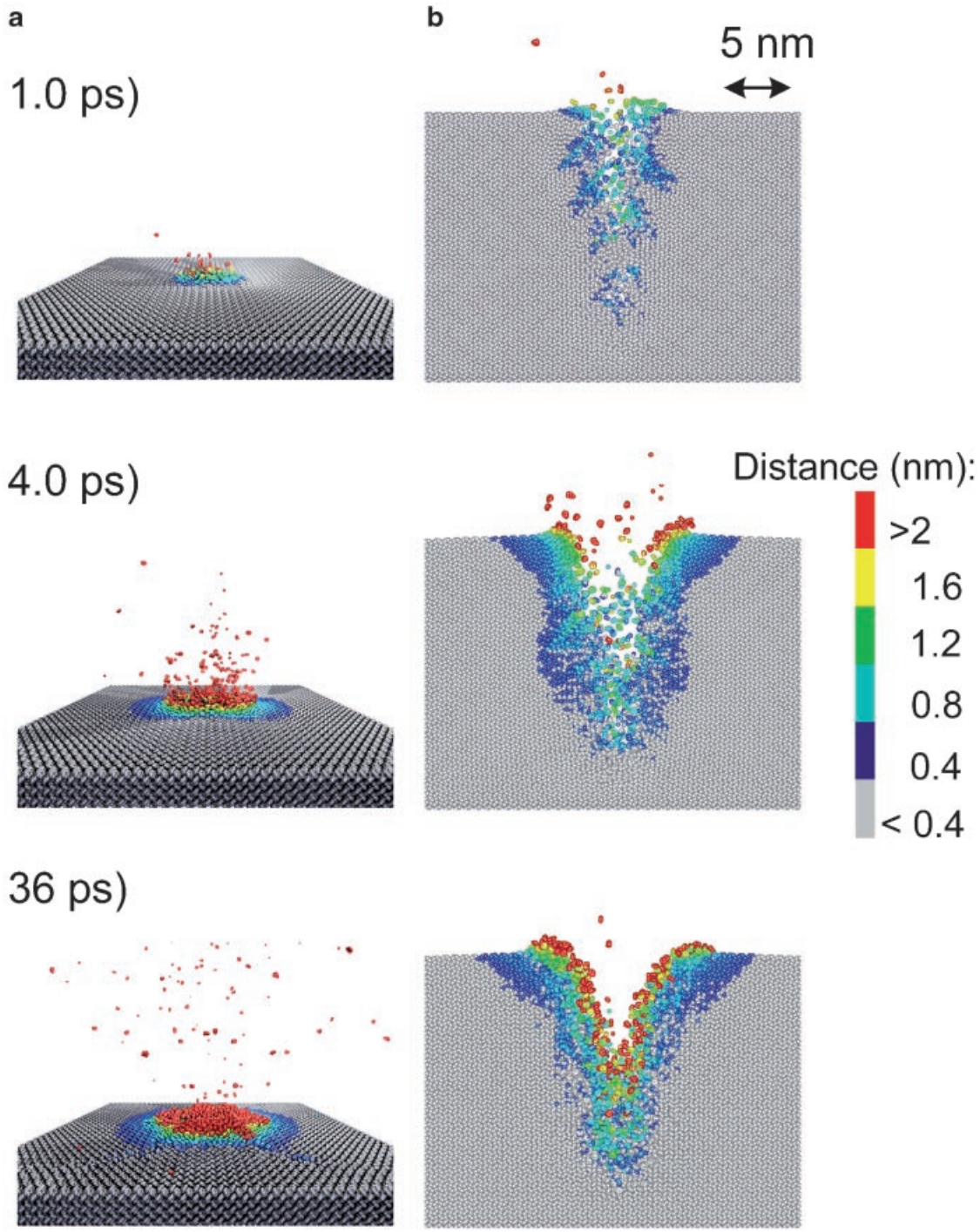

FIGURE 5. Snapshots for 5 keV Au bombardment of solid benzene. **a**: Atomic positions at three times. **b**: A 1.5 nm slice through the center of the sample directly below the impact point. The coloring in both panels is by the amount of displacement from the initial position colored according to the legend on the right side. *Animation 2*. The coloring in the animation is by height where blue is 2.5 nm and deeper into the substrate and red is 2.5 nm or higher above the substrate. The same coloring scheme is used in Animations 5 and 7.

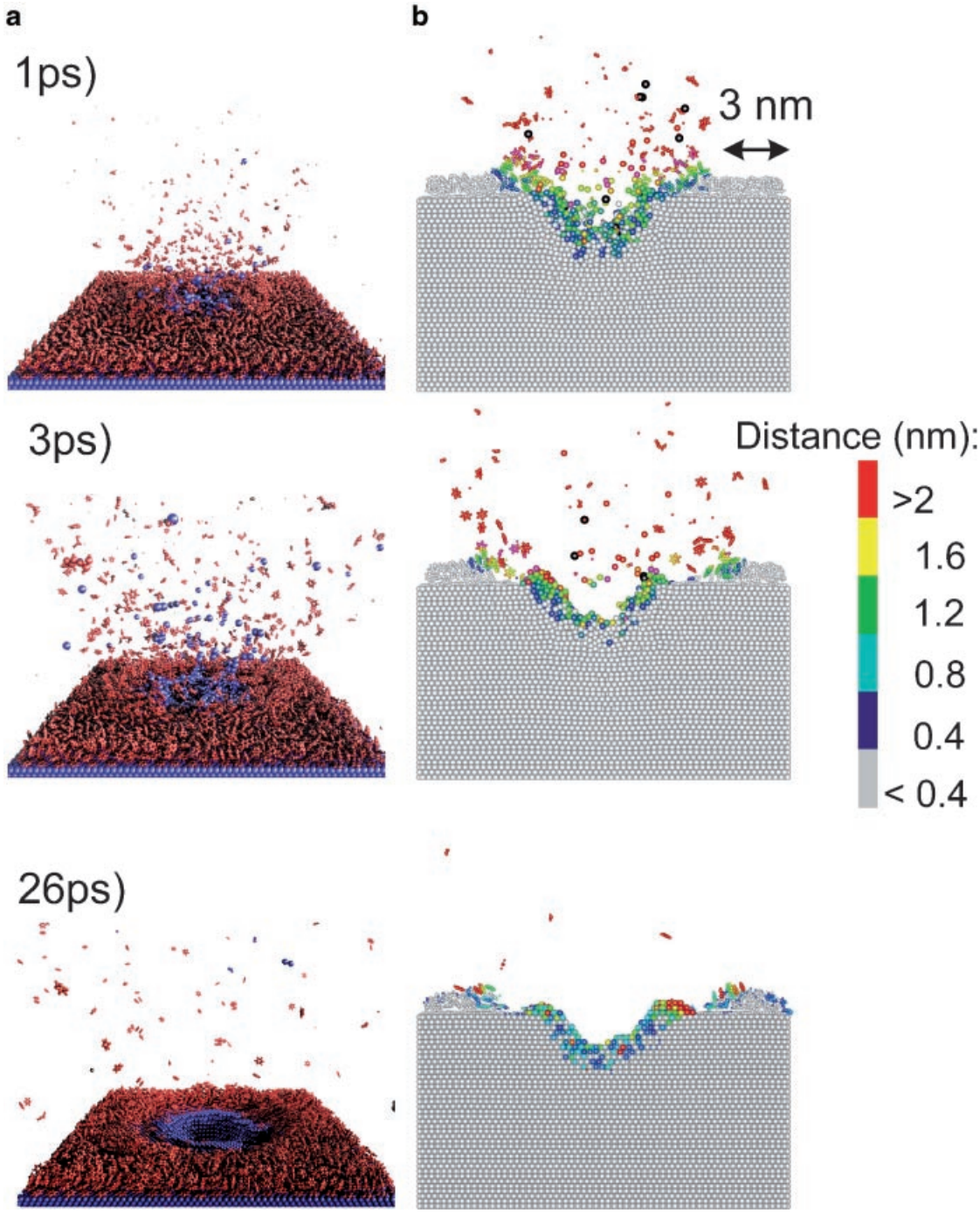

FIGURE 6. Snapshots for 15 keV C_{60} bombardment of three layers of benzene on Ag. **a**: Atomic positions at three times. The coloring scheme is the same as Figure 1a. **b**: A 1.5 nm slice through the center of the sample directly below the impact point. The coloring is by the amount of displacement from the initial position colored according to the legend on the right side. *Animation 3*.

The simulations performed on molecular solids show that both projectiles create craters (Figs. 5 and 8). The atomic crater, however, is more narrow and deeper. The crater formed by C_{60}, on the other hand, is wider and less deep.

In a recent investigation of cluster bombardment of multiple sizes of polymers (Delcorte & Garrison, 2007), several criteria were established for intact molecular ejection. The molecule should not intersect the high-energy core of the projectile track, otherwise reactions occur as discussed below in Section IV.E. The polymer should be entirely confined in the volume that will be displaced (the crater) and it should initially sit in the zone where most of the target atoms receive upward momentum (top

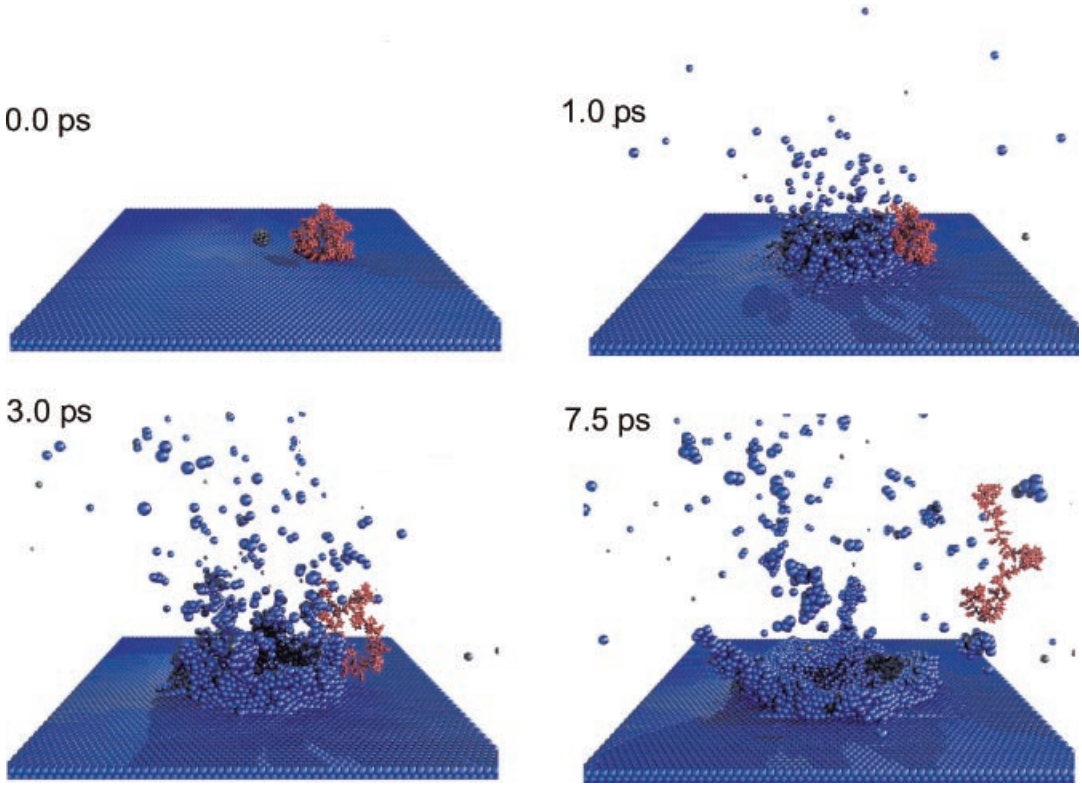

FIGURE 7. Snapshots for the ejection of a polystyrene 61-imer (red spheres) from a Ag surface (blue spheres) due to 20 keV C_{60} bombardment. The PS 61-imer is initially 3 nm from the C_{60} impact point. Only a portion of the Ag substrate is shown. *Animation 4*.

3 nm for 5 keV bombardment). The large-scale nature of the interaction, adequately described using a coarse-grained MD model, explains the large yields of sputtered molecular species usually measured due to keV cluster bombardment of organic materials.

C. Other Fullerene Clusters

The natural question is if C_{60} works so well, might other fullerene clusters (or other types of clusters) work even better. Which cluster size will work the best for a particular system is still being investigated but initial investigations shed some insight. Using the coarse-grained representation of benzene, the ejection yields for a series of clusters from C_6H_6 to C_{180} with 5 keV incident energy were calculated (Smiley et al., 2007). For all the fullerene clusters, they found that the yield was 200–300 molecular equivalents. The maximum yield, however, occurred for an intermediate cluster size, C_{20}. A maximum yield at intermediate cluster sizes has been also observed for other systems (Anders & Urbassek, 2005b). Simulations (Czerwinski et al., 2008; Ryan et al., 2008) and an analytic theory (Seki, Murase, & Matsuo, 2006), however, show that as the incident energy increases the cluster size that gives the largest yield increases. In conclusion, all clusters enhance the yield, some clusters enhance the yield more than the others, and the optimum cluster size depends on the analyzed sample and the incident energy. Regardless of the potentially optimal cluster size, there is always the experimental reality of which clusters can be obtained easily and are cost effectively and which clusters work with experimental beam technology.

D. C_{60} Versus Au_3

A number of cluster beams are being utilized by the experimentalists but C_{60} and Au_3 (or Bi_3) are currently the most popular (Winograd, 2005; McDonnell & Heeren, 2007). These two clusters have similar total mass, 720 amu for C_{60} and 591 (627) amu for Au_3 (Bi_3), but a different number of particles. For the same total energy of the cluster, the energy per particle is smaller for the C atoms versus the metal atoms. There is also a significant difference in the initial size of these clusters. As a result, one might expect different motion of the two clusters in a solid. For illustration, results from simulations of C_{60} and Au_3 bombardment at 5 keV of water ice are shown in Figure 9 (Russo & Garrison, 2006). The heavy Au particles penetrate the ice down to about 10 nm before they come to rest, much like the atomic bombardment simulations discussed above. The C atoms, however, stop within about 4 nm of the surface. Besides the energy per particle difference, the mass of the atoms composing the projectile relative to the target atoms is also important. It is difficult for the light oxygen atoms to deflect and stop the heavy Au atoms. The build-up of Au atoms during repeated bombardment of an organic solid by Au_3^+ projectiles has been observed in experiment (Cheng et al., 2007).

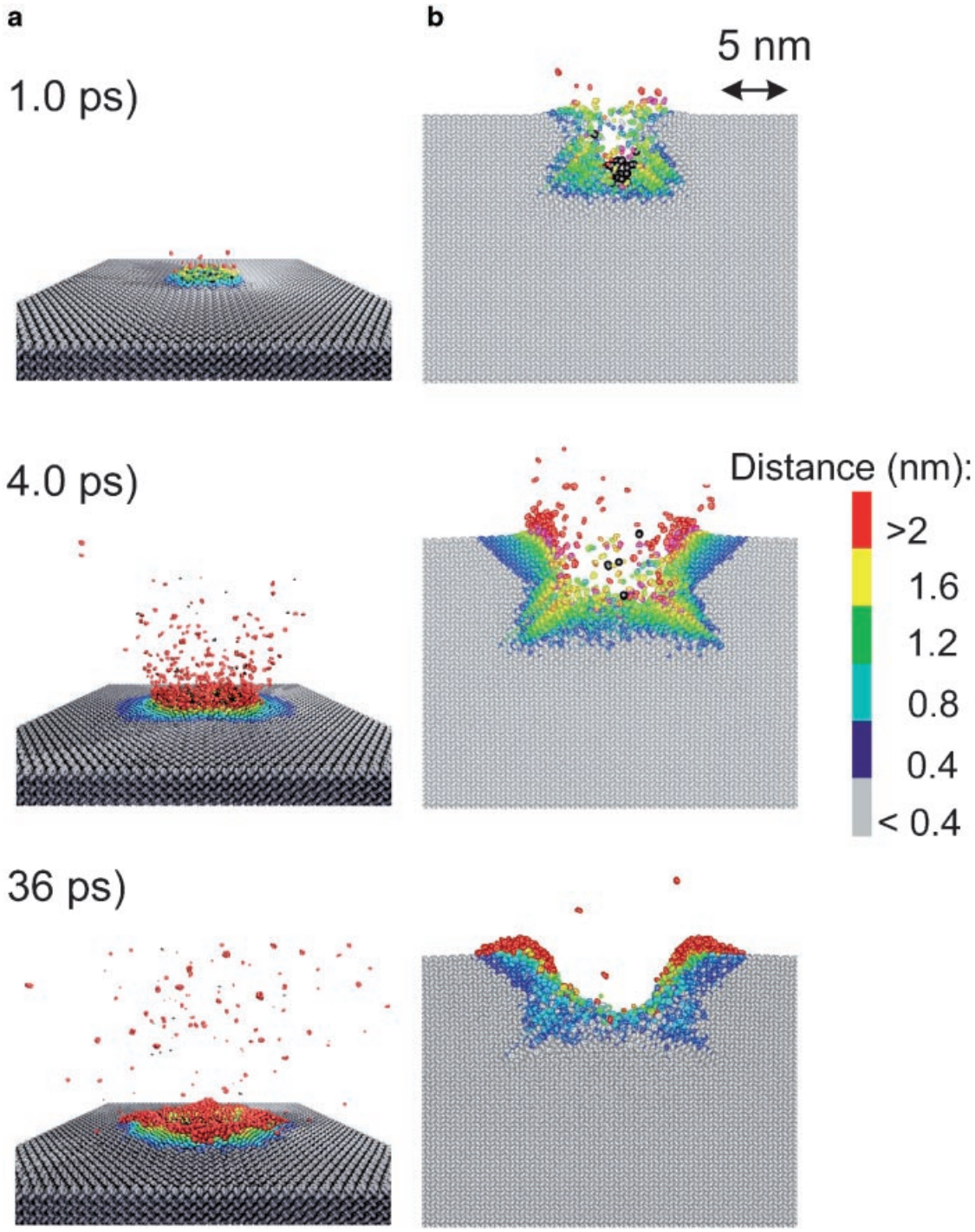

FIGURE 8. Snapshots for 5 keV C_{60} bombardment of solid benzene. **a**: Atomic positions at three times. **b**: A 1.5 nm slice through the center of the sample directly below the impact point. The coloring in both panels is by the amount of displacement from the initial position colored according to the legend on the right side. *Animation 5*. The coloring scheme is described with Animation 2.

Figure 9 also shows the region from which the ejected molecules arise as well as the crater in the molecular solid after 20 psec. For both projectiles, the molecules eject from a conical region of depth approximately 2.5 nm. The conical nature of the ejection volume is a concept we are exploiting by using an analytical model with short-time MD simulations in order to predict yield trends (Russo & Garrison, 2006; Russo et al., 2007). Despite the apparent similarity in the ejection region, the physics is very different for the two projectiles. The Au_3 deposits its energy much deeper than the C_{60} projectile. In fact most of the

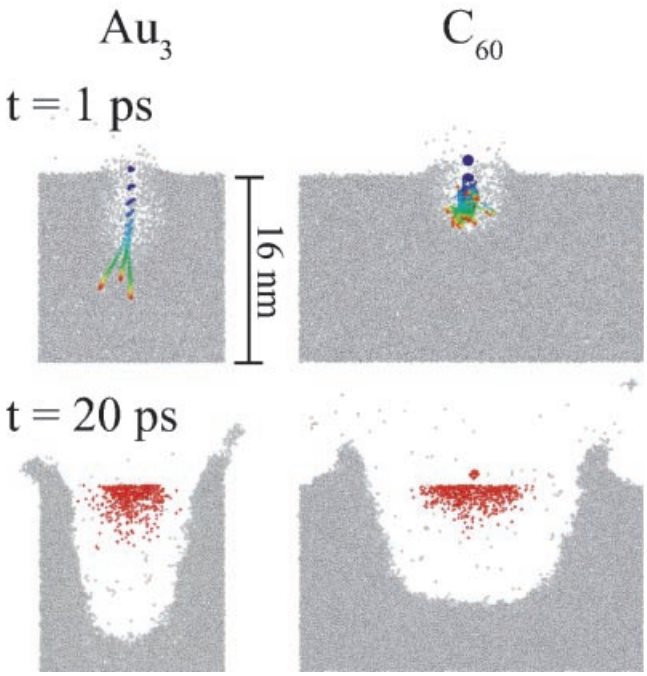

FIGURE 9. Time snapshots of the Au_3 and C_{60} collision events at 1 and 20 psec. Each image is a 2-nm slice through the center of the substrate. Gray dots represent the substrate molecules. The frame at 1 psec contains a time lapse overlay of projectile atomic motion leading up to 1 psec. The colors progress through the rainbow from blue to red with each of the 25 frames separated by 40 fsec. The frames at 20 psec display the ejected particles at their original positions in red overlaid on the substrate at 20 psec. Used by permission from the American Chemical Society, Russo and Garrison (2006).

energy is too deep to contribute effective to the ejection process (Russo et al., 2007). At 20 psec the crater is much larger than the ejected volume. Undoubtedly, with sufficient time, the solid should relax back to the equilibrium density but the process is too time consuming to model.

E. Reactions

Effectively modeling widespread and diverse reactions within molecular simulations is a daunting undertaking. One must have an interaction potential that describes all the possible reaction events. In addition, in SIMS the energies of the collisions can be so high that reaction events for excited state species including ions are also possible, events that cannot be modeled with classical mechanics. We have performed simulations of C_{60} and Au_3 bombardment of water ice for energies between 2.5 and 15 keV, however, using an interaction potential that allows us to monitor whether there is sufficient energy for reactions to occur (Ryan, Wojciechowski, & Garrison, 2007). Snapshots from these simulations are shown in Figure 10. The time of the snapshots is 0.5 psec, a value chosen as when the majority of reaction events have occurred. The gray dots represent intact water molecules in a 2 nm slice of the sample through the center of the substrate below the projectile impact point. The colored spheres represent reacted species whether they are in the slice or not. The

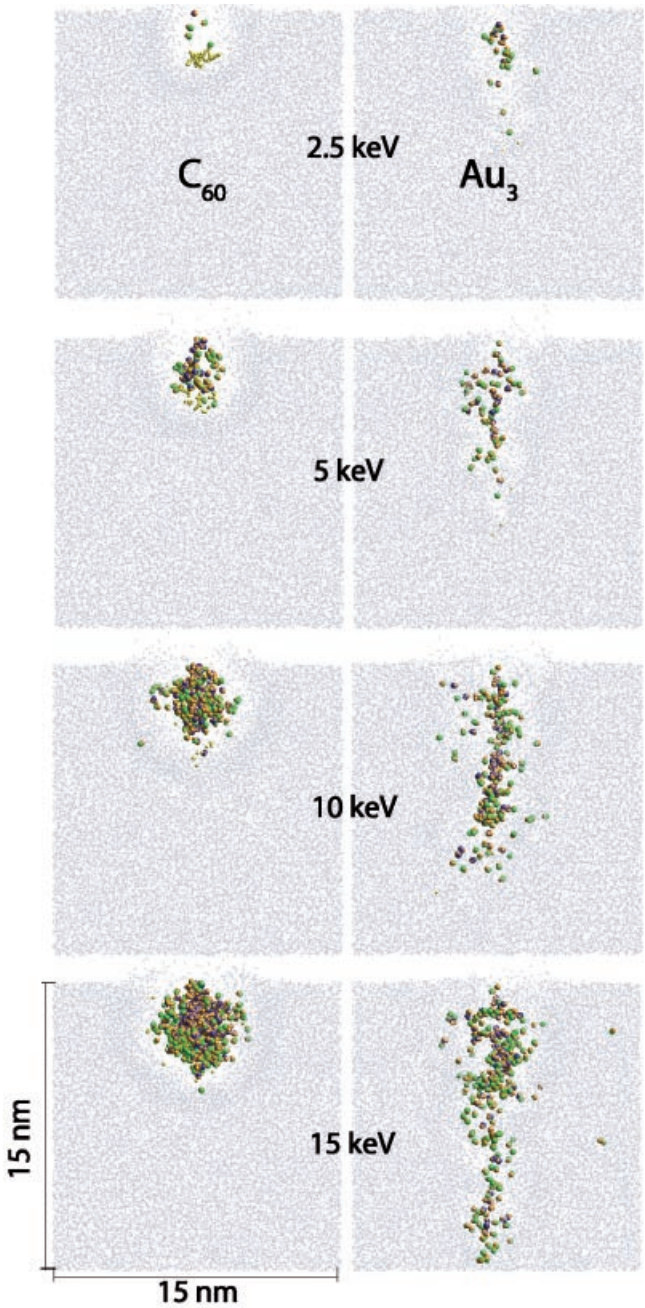

FIGURE 10. Time snapshots of 2.5, 5, 10, and 15 keV C_{60} and Au_3 bombardment of pure amorphous water ice. Gray and yellow spheres represent intact water molecules and projectile atoms, respectively, within a 2 nm slice through the center of the substrate at 0.5 psec. Orange, green, and blue spheres represent the fragment species placed back in their initial positions and overlaid on the substrate at 0.5 psec. Used by permission from the American Chemical Society, Ryan et al. (2007).

fragmented species are placed graphically at their original position in the sample. The positions where the reaction events occur follow the motion of the respective projectiles (Russo, Wojciechowski, & Garrison, 2006). For Au_3 bombardment, as the kinetic energy of the cluster increases, the penetration depth of the Au atoms increases. The fragmented molecules occur

along the motion of the Au particles. There are many occurrences of individual dissociated molecules, although there are some regions in which several nearby molecules have fragmented. In contrast to the Au atomic motion, the C atoms from the fullerene cluster stop within 4–5 nm of the surface. Thus, the reaction events are confined to a very dense region near the point of impact. The number of reacted molecules exhibits a non-linear increase as a function of increasing projectile energy, indicating that there is cooperation among the motion of the C atoms in terms of influencing the reaction probability. The nature of the reaction environment for C_{60} bombardment, especially at the higher incident energies, is quite different. The reaction rate is greatest at about 100 fsec when a crater under the impacting C_{60} particle has started to form. The molecules initially in the volume where the crater has formed have been compress into the bottom and sides of the crater formatting a dense region. It is within this dense and highly energized region that the reactions are occurring. These simulations strongly suggest that multiple atoms/molecules are simultaneously involved in the reactions initiated by cluster bombardment, especially for C_{60} particles. In addition to the compressed geometrical region, the events are occurring in a very short time frame, thus many non-adiabatic and excited state reactions are energetically possible. This massive motion could spawn any number of complex reaction or ionization events.

F. Implications for 2D Imaging, Depth Profiling, and 3D Imaging

The excitement with cluster bombardment in SIMS is an enhanced brightness of the signal in 2D imaging experiments, molecule specific depth profiling, and the combination of the two, that is, 3D imaging (Fletcher et al., 2007; Wucher, Cheng, & Winograd, 2007). [A review of molecular imaging experiments in general has recently appeared in this journal (McDonnell & Heeren, 2007)]. The simulations highlight some important differences between cluster bombardment and atomic bombardment. First, every cluster hit ejects about the same amount of material. There are no winners and losers as with the ions in atomic SIMS, for example, see Figure 2. Second, the amount of material ejected is much larger than with atomic SIMS. Experiments for Au^+ at 25 keV and C_{60}^+ at 20 keV bombardment of water ice have yields of 94 and 1,830 molecular equivalents, respectively (Szakal et al., 2006). Calculations of 15 keV Ga and C_{60} bombardment of a silver substrate predict yields of 21 and 327, respectively (Postawa et al., 2004). The larger yield [and ion yield (Weibel et al., 2003)] of material and consistent yield from each ion hit makes the 2D images brighter. Second, the simulations show clearly that there is less displacement in the substrate with the C_{60} bombardment than atomic bombardment, that is, compare Figure 6 with Figure 3 and compare Figure 8 with Figure 5. Our simulations that allow reactions (i.e., damage) (Ryan et al., 2007) as presented in Figure 10 show that the reactions are confined to a smaller volume than the total displacements, thus the damage region for the trajectory shown in Figure 8 is even less than the colored region. The crater volume is greater than the damage region, thus the next hit has the potential to remove a majority of the damaged molecules and sample a considerable amount of unaltered volume, ideal conditions for molecular depth profiling (Cheng, Wucher, & Winograd, 2006). The MD simulations provide a graphic and clear understanding of why cluster beams such as C_{60} make 2D imaging, depth profiling and 3D imaging experiments possible in SIMS.

V. ATOMIC VERSUS CLUSTER BOMBARDMENT OF THIN AND THICK FILMS OF WATER ICE ON SILVER

The principles we have discussed for atomic and cluster bombardment on thin and solid films of organic molecules can be used to interpret SIMS data for Au^+, Au_2^+, Au_3^+, and C_{60}^+ bombardment of water films of varying thickness on a Ag surface (Szakal et al., 2006). The measured quantity is the Ag^+ signal as a function of water thickness as shown in Figure 11 for the four projectiles. The signals follow a near-exponential decay with the signal from C_{60}^+ bombardment decaying most quickly with water thickness and the signal from Au^+ bombardment the slowest.

The obvious questions are first, why is there a difference with projectile, and second, what does it mean to have a Ag^+ ion 'escape' from a water film of 10–20 nm. The answer to the first question is illustrated by the snapshots in Figures 3, 5, 6, 8–10. The C_{60} deposits its energy in the top 4–5 nm of the water film. Once the film thickness exceeds this dimension, the C_{60} cannot impart energy to the underlying Ag substrate in order to eject Ag atoms. A water film thickness of about 5 nm is sufficient to eliminate the Ag^+ signal. (Of note, Figure 9 is for 5 keV bombardment at normal incidence, Figure 10 goes up to 15 keV whereas the experiment in Figure 11 is for 20–25 keV bombardment at 40–45° incidence. The data may vary but the concepts presented here are applicable to the higher energies.) The Au_3, on the other hand can penetrate deeper into the film by a factor of 2–3 more than the C_{60}, and the Au even further. The deeper the projectile can penetrate, the thicker a water film is needed to inhibit the ejection of Ag^+ ions.

The second issue that the simulations can answer is what it means for a Ag^+ ion to eject from an overlayer film. One explanation might be to say that the Ag particle escapes through the water overlayer. It is hard to conceive, however, of a sputtered particle with only several eV of kinetic energy being able to penetrate a several nanometer film of water. The key dynamics is seen in Figures 3,6 and 12. In particular, Figure 12 displays the dynamics of Au_3 and C_{60} bombardment at 15 keV of a 2.5 nm film of water on Ag. The projectile in all cases is able to clean the surface of overlayer film, thus providing an open escape route for sputtered Ag particles.

This example of Ag^+ ion intensities as a function of water overlayer thickness demonstrates the power of the MD simulations to help interpret experimental SIMS data. Not only are the relative trends versus projectile type explained but also the reason that Ag can eject from a seemingly 'thick' overlayer of several tens of nm. The observation of metal atoms ejecting in the presence of a thick organic layer is not unprecedented. Bolbach et al. (1988) deposited Cd stearate Langmuir-Blodgett layers on Au and Ag substrates and measured the substrate ion signal due to 21 keV Cs^+ bombardment as a

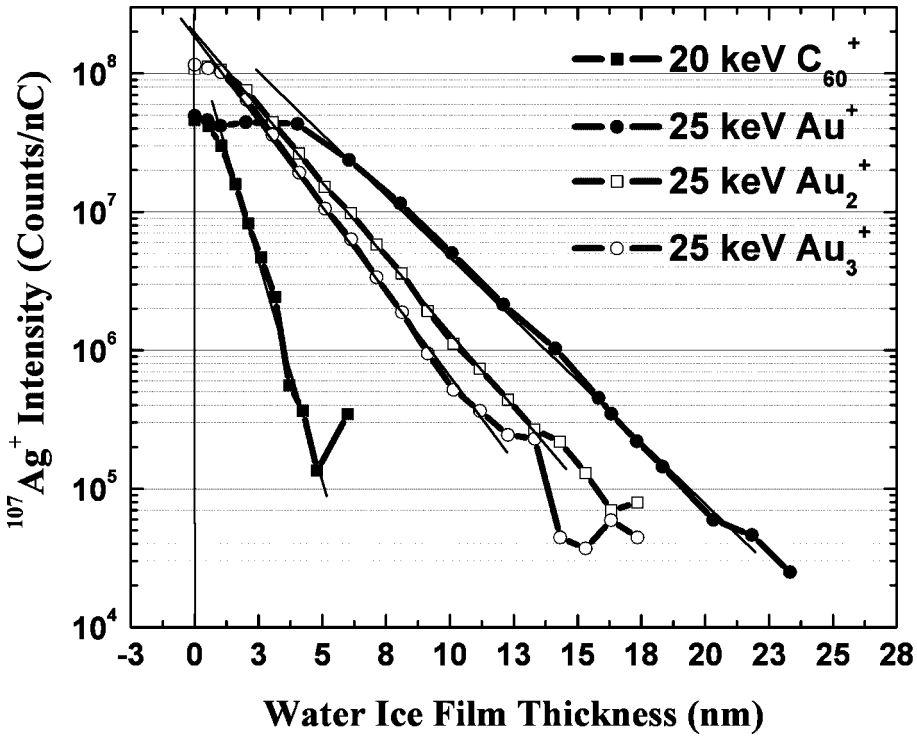

FIGURE 11. Experimental $^{107}Ag^+$ ion intensity versus water ice film thickness for the four primary projectiles being studied. Linear regression lines for the central portion of each curve are included. Used by permission from the American Physical Society, Szakal et al. (2006).

function of coverage. They found that there is a measurable Ag^+ ion signal to 8 layers or about 20 nm. Wong, Lockyer, and Vickerman (2005) measured the emission of Au^-, Au_2^-, and Au_3^- from thiolate layers adsorbed on a Au substrate due to 25 keV Ga^+ bombardment. For the Au^- emission they find a depth of origin of 7 nm and see emission of all three ions up to a depth of 10 layers or 16 nm. The mechanism proposed from the MD simulations suggests that the metal ions are not ejecting through the overlayer but rather the overlayer is swept away providing an unimpeded path for ejection.

VI. LARGE CLUSTER BOMBARDMENT

If clusters like SF_5, Au_3/Bi_3, and C_{60} are better than atomic projectiles, does that mean that bigger is even better? If so, how much bigger is better? Increasing the size of the cluster enormously, in fact, can make for extremely large total energies even for a small energy per particle. For example in DESI, the energy per molecule in the cluster is sub meV, but since it is a micron size particle, the total energy is GeV (Takats et al., 2005). For clusters of the size of several hundred to several thousand particles, the beam sources are primarily in one or two labs and are not commercialized for mass spectrometry applications. Rather the application has been predominantly surface smoothing (Yamada et al., 2003) and consequently the simulations have been limited to rare gas cluster bombardment of atomic samples (Aoki et al., 2001, 2003; Aoki & Matsuo, 2006). Atomistic simulations of DESI, in fact, may be currently intractable. Thus, this section contains a brief overview of the first studies of large cluster bombardment of thin organic layers on a metal substrate (Rzeznik et al., 2008) and one trajectory of a large cluster bombardment of a molecular solid.

A. Thin Organic Layer

Two energy regimes have been identified for ejection of organic molecules from a metal substrate due to large cluster bombardment (Rzeznik et al., 2008). The first regime is when the cluster has sufficient energy to create a crater in the metal substrate and then the subsequent motion is similar to C_{60} bombardment as discussed above. The distinctive regime is when the energy of the cluster is sufficiently low that no displacements are created in the metal substrate as shown in Figure 13 and *Animation 6* for an Ar_{9000} cluster with 18 keV bombarding a layer of polystyrene tetramers (PS4) on Ag. The molecules are removed from a ring-like region and no substrate Ag atoms are displaced. Lowering the incident kinetic energy by a factor of four results in no ejection of PS4 molecules. In these simulations, the PS4 molecule is bound by about 2.1 eV to the substrate. Thus, there is an intermediate energy regime where molecules can be ejected without damage to the substrate. Two new mechanisms of emission have been identified from the simulations. The first is a mechanism that ejects molecules from the edge of the incident cluster almost like washing them from the surface and the second is a compression mechanism for molecules directly under the cluster.

The washing mechanism is illustrated in Figure 14 where the key action occurs along the direction that contains the red, green, and black PS4 molecules. The incident cluster in a continuous, collective motion pushes the red molecule sideways and towards

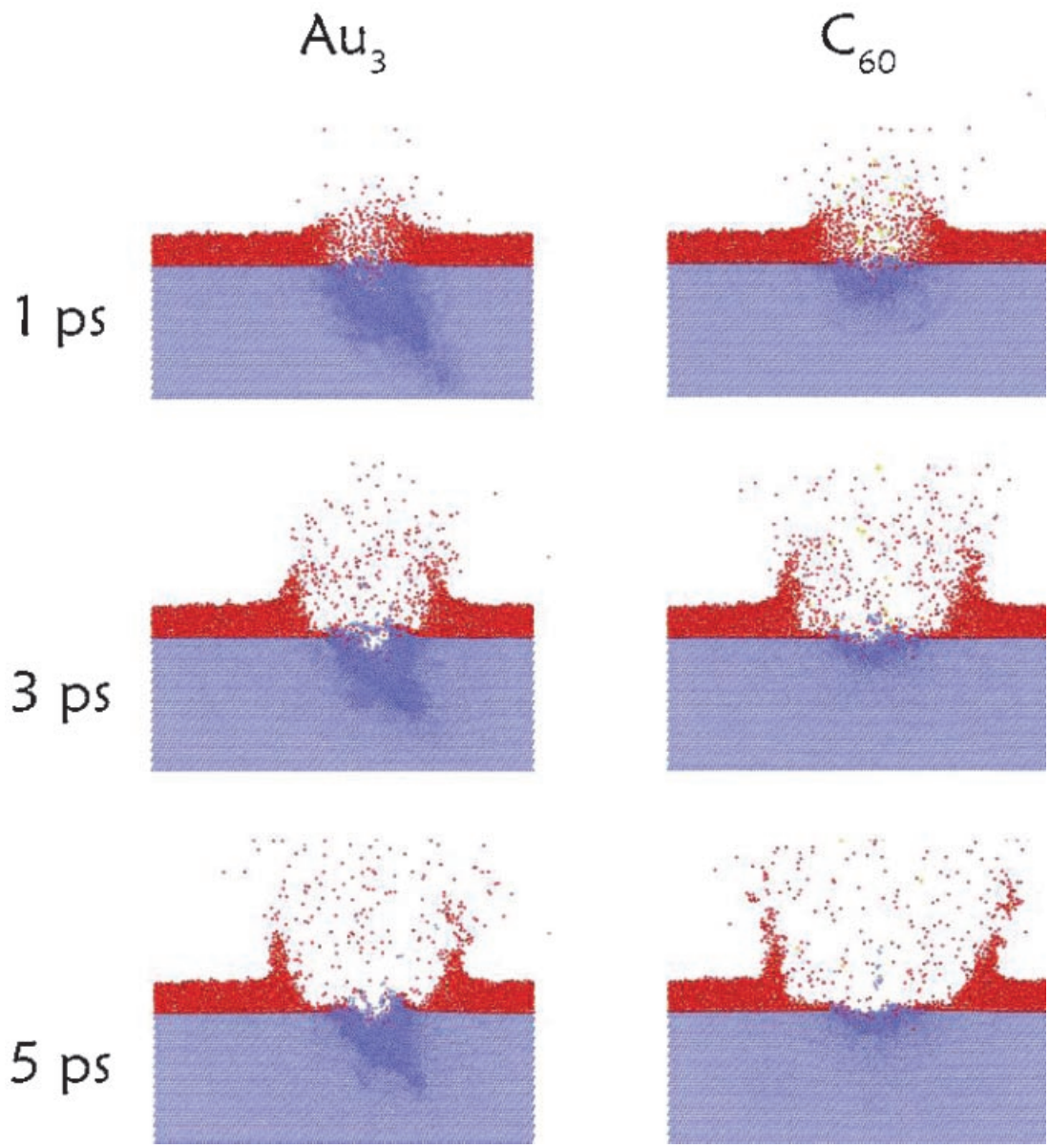

FIGURE 12. Snapshots of the atom positions for Au_3 and C_{60} bombardment of a 2.5 nm film of ice (red) on Ag (blue). The incident particle impinges from the left with 15 keV at an angle of 40° with respect to the surface normal. The time snapshots are at 1, 3, and 5 psec for the frames from top to bottom, respectively. Used by permission from the American Physical Society, Szakal et al. (2006).

the metal substrate. As the red molecule is pushed sideways and down, the Ag substrate and the green molecule exert an upward force. The red molecule ejects with 52 eV of kinetic energy. This motion now proceeds in a chain with the green molecule being pushed down and sideways until the Ag substrate and the black molecule exert an upward force. The green molecule ejects with a smaller amount, 31 eV, of kinetic energy. In general, the number of molecules ejected with the Ar cluster is larger than with C_{60} bombardment and the ejected molecules have much larger kinetic energies. In addition, due to specific properties of ejection process, the angle of emission is peaked near grazing angles.

As shown in Figure 13 most of the molecules are ejected from a ring-like area starting close to the perimeter of the Ar cluster *via* mechanisms similar to those shown in Figure 14. Surprisingly, there is almost no ejection from the area located below the cluster. Even if a molecule does obtain sufficient upward energy by being pressed down by the cluster and up by the surface, the molecule must penetrate the cloud of Ar atoms above it in order to eject. As a result, the ejection by this channel can only occur very late in the trajectory as shown in Figure 15 and the ejected molecules have relatively small amounts of kinetic energy. The recovering substrate atoms are responsible for propelling the blue PS4 molecules into the vacuum.

The observations provide insight into the efficacy of slow, large noble-gas cluster beams for molecular desorption in TOF-SIMS experiments. There are several features which indicate that

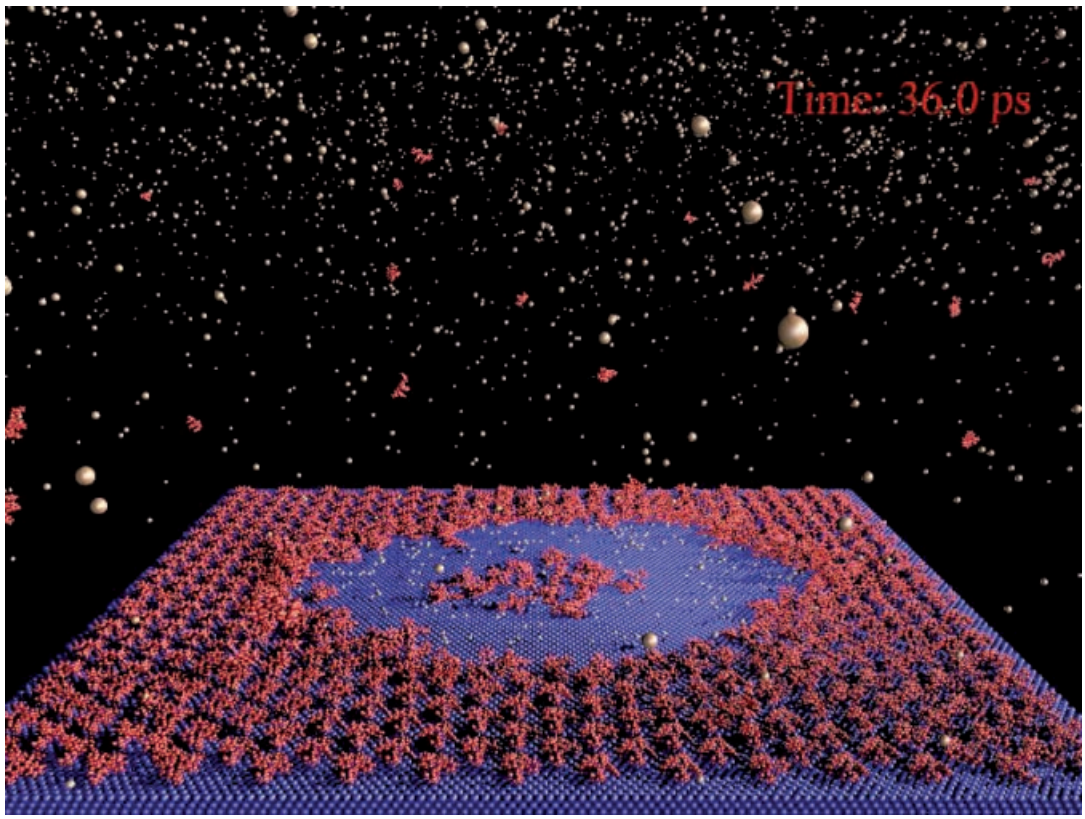

FIGURE 13. Final time snapshot for 18 keV Ar_{9000} bombardment of a layer of PS4 on Ag. The blue spheres represent Ag atoms, the red spheres are C and H atoms in the PS molecules and the peach color spheres are the Ar atoms. Used by permission from the American Chemical Society, Rzeznik et al. (2008). *Animation 6*.

application of such projectiles could be potentially useful for SIMS/SNMS analysis of thin organic overlayers deposited on an inorganic substrate. First, a large molecular signal is generated by the impact of a single projectile. This observation differs from measurements performed with small cluster projectiles where signal is usually low and no significant yield enhancement is reported when the atomic projectile is replaced by a small cluster ion (Weibel et al., 2003; Sostarecz et al., 2004; Winograd, 2005). The efficiency of molecular ejection increases with the size of the cluster provided that a constant energy per atom can be secured. At the same time, the onset for molecular desorption is shifted towards a lower kinetic energy per atom. Lowering of the desorption threshold results in ejection of less internally excited molecules and, consequently, to a lower fragmentation of molecules on their way to the detector. All these observations indicate that a primary beam composed of the largest available clusters should be used to probe organic overlayers. Bombardment by a larger cluster results also in a larger number of Ar atoms having a chance to collectively interact with the organic molecule. A cumulative action of a larger number of projectile atoms should, in turn, allow uplifting of larger molecules. As a result, application of such projectiles could potentially allow detection of higher molecular weight molecules (Cornett et al., 1994). Another potentially positive feature of large cluster ion beams is the ability to collect spectra without fragments (Rzeznik et al., 2008). This ability could in some cases simplify the procedure of chemical identification of analyzed material. However, if the presence of specific fragments is necessary to accomplish more elaborate chemical identification, it can be achieved by a simple increase of the kinetic energy of the primary beam.

B. Organic Solid

The time snapshots from 5 keV Ar_{872} bombardment of the coarse-grained benzene system are shown in Figure 16 and *Animation 7*. For comparison the results of 5 keV atomic bombardment and 5 keV C_{60} bombardment are shown in Figures 5 and 8, respectively. The general behavior of Ar cluster is similar to the behavior of C_{60} cluster and is different from the behavior observed during bombardment of thin organic overlayers on metal substrate. After the impact on the benzene crystal, the projectile easily penetrates into the organic sample due to its low cohesive energy. Due to the softness of the organic substrate, formation of a high-density, high-pressure region at the sample/cluster interface is less probable as compared to the impact on the hard metal substrate. As a result, the propagation of a shock-wave inside the projectile which led to a side jetting of projectile atoms is greatly reduced. As seen in the snapshot collected at 1 psec, the Ar atoms are surrounded by the organic material. At 36 psec most of the projectile atoms are back-reflected into the vacuum and a large crater is formed in the

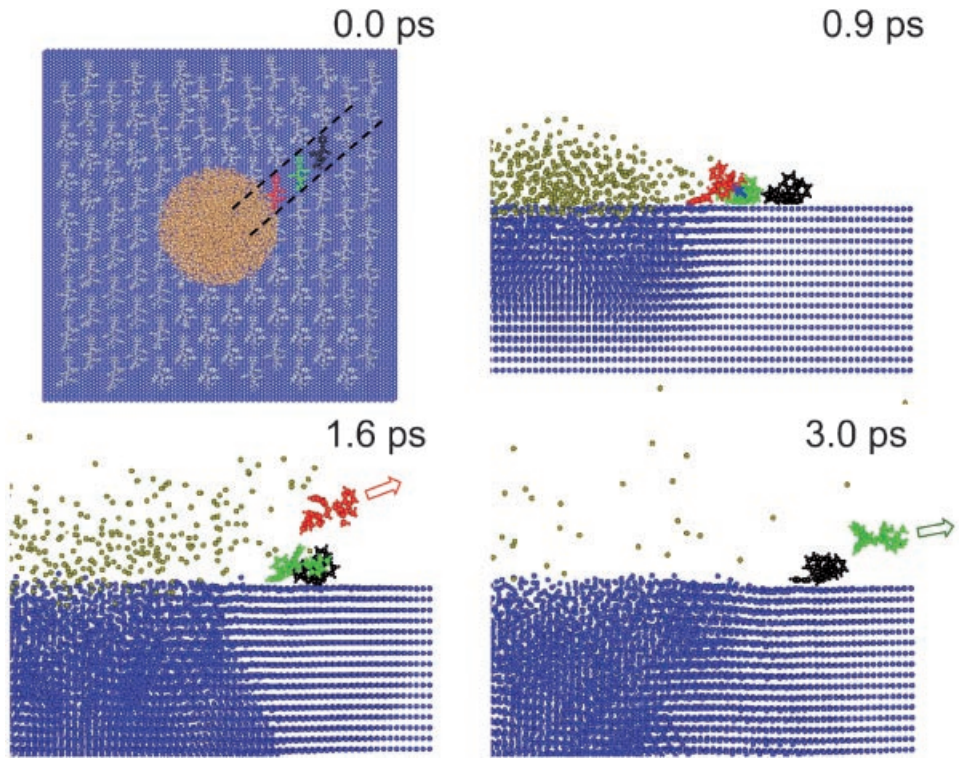

FIGURE 14. Time evolution of the ejection of high- and medium-energy PS4 molecules induced by 15 keV Ar_{2953} cluster impact at normal incidence. A top view is shown at the initial time. The subsequent times display particles located within a slice 1.6 nm wide centered at the point of impact. The orientation of the slice is schematically marked by dashed lines in the topmost panel. Only molecules involved in the mechanism discussed in the text are shown. The arrows indicate the final direction of momentum of ejected PS4 molecules. Used by permission from the American Chemical Society, Rzeznik et al. (2008).

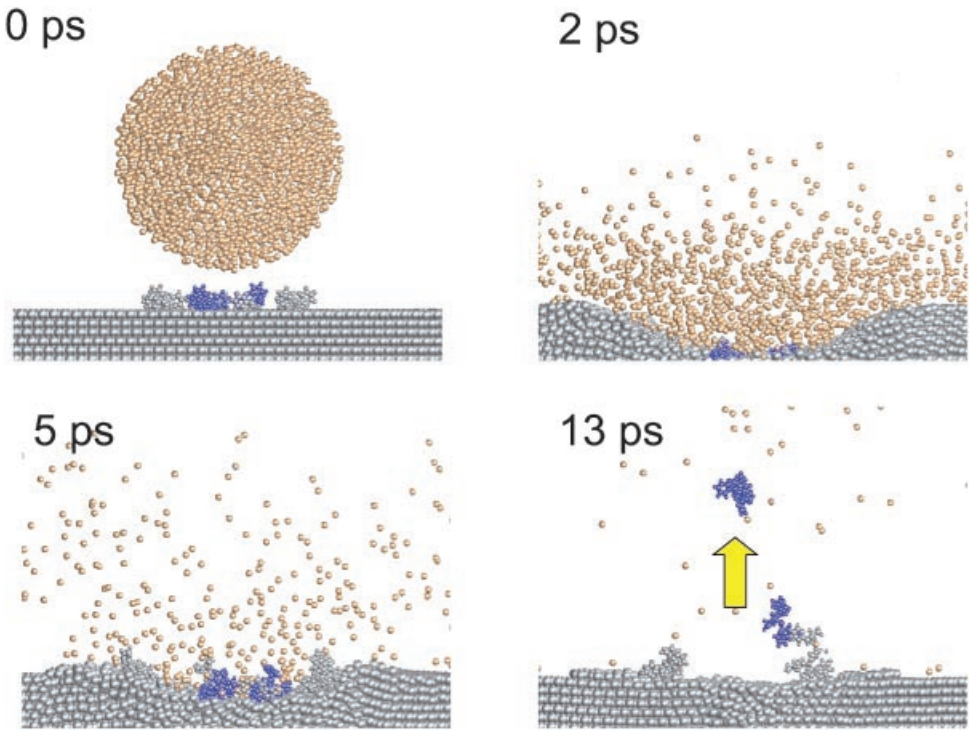

FIGURE 15. Time evolution of the ejection of low-energy PS4 molecules induced by 15 keV Ar_{2953} cluster impact at normal incidence. Only ejected molecules together with their nearest neighbors located within a slice 1.5 nm wide centered at the point of impact are shown. Used by permission from the American Chemical Society, Rzeznik et al. (2008).

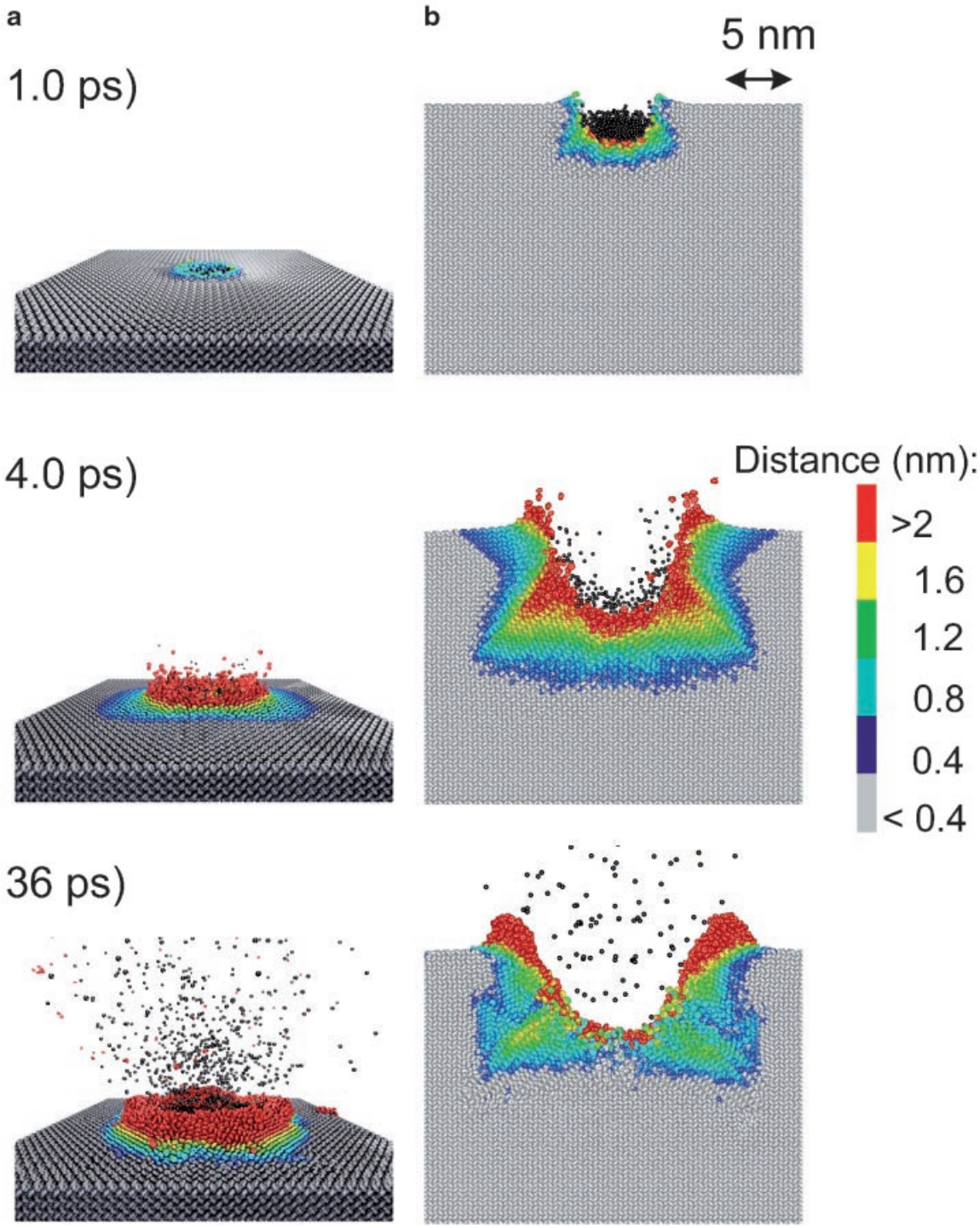

FIGURE 16. Snapshots for 5 keV Ar_{872} bombardment of solid benzene. **a**: Atomic positions at three times. **b**: A 1.5 nm slice through the center of the sample directly below the impact point. The coloring in both panels is by the amount of displacement from the initial position colored according to the legend on the right side. *Animation 7*. The coloring scheme is described with Animation 2.

sample. The size of the crater is larger than for 5 keV C_{60} irradiation. However, this difference is not caused by a larger sputtering yield but by a larger material compression factor induced by an impact of heavier projectile (Russo & Garrison, 2006). In fact, the calculated total sputtering yield for 5 keV C_{60} impact is 317 molecules, while barely 97 molecules are emitted by 5 keV Ar_{872}. Such a low sputtering yield induced by Ar cluster is a consequence of the primary energy being deposited too

shallow as discussed in the Section IV.C. The same processes seem to lead to ejection of benzene molecules by both C_{60} and Ar_{872} projectiles. Some differences may occur at higher impact energy where the importance of the effect of the substrate softness diminishes and the formation of the shock wave in the deforming projectile is more probable. However, no calculations have been done so far at this energy range to confirm this supposition.

VII. MALDI

The length and time scale of MALDI or laser ablation far exceeds what can be modeled with conventional atomistic MD simulations. The laser probe size is tens of microns in diameter, the UV radiation of typical UV MALDI matrices is absorbed in a several tenths of micron depth and the laser pulse with of N_2 lasers lasts a handful of nanoseconds. To put this volume in perspective, assume a 20 μm diameter of the laser probe, a 0.2 μm ejection depth and a density of the matrix of $1 g/cm^3$. The amount of material ablated is approximately 6×10^{-11} g. For C_{60} bombardment of water ice at 20 keV, the amount of material removed is 1,830 water molecule equivalents (Szakal et al., 2006) or 5×10^{-20} g. There is a factor of nine orders of magnitude in volume of removed material for these two techniques. The difference in timescale of the important motion is a factor of a thousand larger for UV MALDI than cluster bombardment. To apply the same simulation approach for MALDI as with cluster bombardment is impossible. To make progress in understanding the ejection process, therefore, a strategy was developed to make sure the essential physics/chemistry was incorporated while at the same time omitting compute intensive, not-as-essential aspects (Zhigilei et al., 1997, 1998; Zhigilei & Garrison, 2000; Zhigilei et al., 2003a,b; Leveugle & Zhigilei, 2007).

The size of the simulation system is restricted in all dimensions after carefully assessing the important physics. Only the system in the center of the laser probe is considered with periodic boundary conditions applied. For the example discussed here (Leveugle & Zhigilei, 2007), a sample of width 40 nm is used as shown in Figure 1d. The penetration depth, a quantity inversely proportional to the absorption coefficient, used is 50 nm. Careful application of a pressure absorbing boundary condition (Zhigilei & Garrison, 1999b) allows the system to be only 60 nm deep. The laser pulse width is 50 psec, a time sufficiently long that the physics of ablation is by the same physics as in the MALDI experiments (Zhigilei & Garrison, 2000). Finally, a coarse-grained approach was used in which each matrix molecule was approximated by one particle in the simulation (Zhigilei et al., 1997, 1998). This last approximation allows for an order of magnitude fewer particles and a simpler interaction potential for which a larger time step in the numerical integration can be used.

The novel feature of the coarse-grained description of the matrix molecules is an internal breathing mode for each particle (Zhigilei et al., 1997, 1998). This breathing mode is used for depositing the energy of the incident photon as kinetic energy. The parameters of the interaction potential for the breathing mode are chosen to give a reasonable rate of energy transfer to the remaining solid. The use of the breathing mode circumvents the whole issue of how the photons get absorbed into the electronic state and then redistributed to vibrational motion. The concept is that this process does happen, and the simulations only model what happens afterwards. Because there is a mechanism for depositing the photon energy into the matrix, an explicit pulse width, Beer's law dependence, and fluence can be included. Matrix molecules are randomly chosen within the appropriate time and spatial dependence of interest for absorbing a photon of energy. Analyte molecules of mass 10 kDa are described by a chain of coarse-grained particles of the same size as matrix molecules bonded together by potentials appropriate for a C–C bond (Leveugle & Zhigilei, 2007). The analyte molecules can dissociate if the forces on them are sufficiently strong.

The predicted yields as a function of fluence are shown in Figure 17 for a system of pure matrix molecules (Zhigilei & Garrison, 2000; Zhigilei et al., 2003b). There is an initial increase in yield with fluence at low fluence, followed by a discontinuous jump in yield followed by an additional increase in yield. In the low fluence regime, the simulations show quite clearly that the physics of material removal is desorption of primarily individual molecules. The calculated yields are described well by a model in the literature based on a thermally activated process (Dreisewerd et al., 1995; Johnson, 1996; Zhigilei & Garrison, 1999a). At fluences above the point where the discontinuous jump in yield occurs, that is, the ablation threshold, the physics that gives rise to the ejected material is based on a volume removal model (Srinivasan & Braren, 1989; Johnson, 1996; Zhigilei & Garrison, 1999a) and the plume has a different character. The plume consists not only of individual molecules but also large clusters of matrix molecules. It is the presence of the clusters that characterizes the ablation process. The laser heats the matrix sufficiently quickly that the temperature reaches approximately 90% of the critical temperature (Garrison, Itina, & Zhigilei, 2003). At this point, the incubation period for the onset of the homogeneous boiling drops from more than a nanosecond to picoseconds as the temperature increases by ∼1%.

One prediction of the simulations is that in the desorption regime there are no large clusters of molecules, right above the threshold the clusters are largest and at higher fluences they are smaller. This prediction has been verified in experiments in which the ejecta is collected on a glass slide and then imaged with atomic force microscopy as shown in Figure 17. At the lowest fluence they do not observe clusters, at a moderate fluence they observe the largest clusters and at a higher fluence the clusters are smaller. These clusters are of a variety of sizes and would comprise a background signal in any MALDI experiment.

The physics of ablation, that is, absorption of energy in a volume near the surface followed by a phase explosion, involves a coordinated motion of large amounts of material towards the vacuum. Several simulations (Zhigilei & Garrison, 1998; Sadeghi, Wu, & Vertes, 2001; Yingling et al., 2001; Itina, Zhigilei, & Garrison, 2002; Kristyan, Bencsura, & Vertes, 2002; Leveugle & Zhigilei, 2007) show that large or non-volatile analyte molecules only eject above the ablation threshold and that they do not eject in the desorption regime. An example of ablation with an analyte molecule incorporated is shown in Figure 18 and *Animation 8*. The coloring scheme clearly distinguishes between the analyte molecules that eject (green)

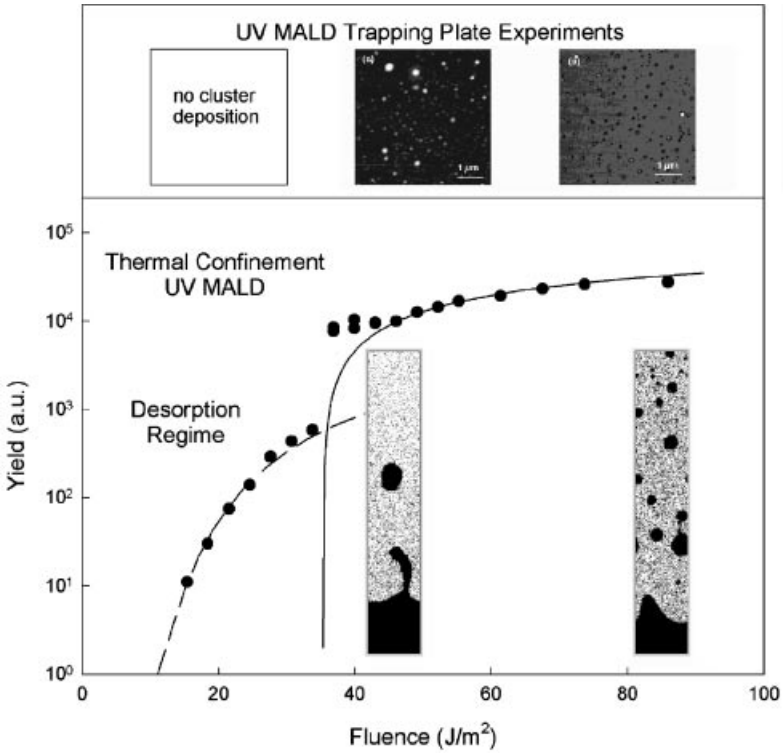

FIGURE 17. Total yield as a function of laser fluence. The lines represent predictions of models as discussed in Zhigilei et al. (2003b). Included are snapshots from the simulations just above the ablation threshold (39 J/m^2) and at 1.75 times threshold (61 J/m^2). The frames at the top show the results from trapping plate experiments (Handschuh, Nettesheim, & Zenobi, 1999) for fluences of 20, 40, and 120 J/m^2, from left to right. No clusters or analyte molecules are detected at 20 J/m^2, whereas molecular films of 1 and $\sim$20 nm thickness speckled with clusters are found to cover the trapping plate at 40 and 120 J/m^2, respectively. Simulation data are from Zhigilei and Garrison (2000). Used by permission from Elsevier, Zhigilei et al. (2003b).

and those that do not (red). All of the ejected analyte molecules are in the part of the matrix that ablates (yellow). It is the collective motion or phase explosion (Zhigilei & Garrison, 2000; Garrison et al., 2003) that provides the thrust to lift off the heavy, non-volatile molecules. Because MALDI (laser ablation) involves a collective motion of a large (almost macroscopic) amount of material, it is not surprising that the largest molecules observed in MALDI are at least an order of magnitude larger than those observed in SIMS.

The simulations of analyte ablation from within a matrix (Zhigilei & Garrison, 1998; Sadeghi et al., 2001; Yingling et al., 2001; Itina et al., 2002; Kristyan et al., 2002; Dou et al., 2003; Leveugle & Zhigilei, 2007) consistently predict that the analyte molecule should be solvated by matrix molecules. In other words, if large analyte molecule is present then it participates in the clusters and is solvated. The amount of solvation is decreased if the analyte molecule is near the surface or if the laser fluence is high but the solvation never quite goes away (Itina et al., 2002; Zhigilei et al., 2003b; Leveugle & Zhigilei, 2007). It is thus perplexing how the isolated analyte ion signal appears so clearly in MALDI experiments. Our experience in performing MD simulations indicates that they are well designed and that the interaction potentials are sensible. Obviously, a renewed effort needs to be made to understand the desolvation of the analyte molecule.

VIII. IONIZATION

The MD simulations give an exquisite view of the motion of the particles following bombardment by energetic particles and laser irradiation. A plethora of results from the simulations have given tremendous insight into surface based mass spectrometry. The big missing link between the results from simulations versus experiment is the ionization process, as it is ions that are detected. In SIMS and MALDI these ions are formed before or during the energizing event and removal from the surface and are not formed by any means of experimental postionization procedure.

The predominant parent ions in both SIMS and MALDI for organic and biological samples are $(M \pm H)^{\pm}$ where M is the molecule of interest. Ions in which the molecule is attached to species such as Na^+, K^+, Ag^+, or Au^- are also observed. There are two simulation studies which illustrate the beginning stages

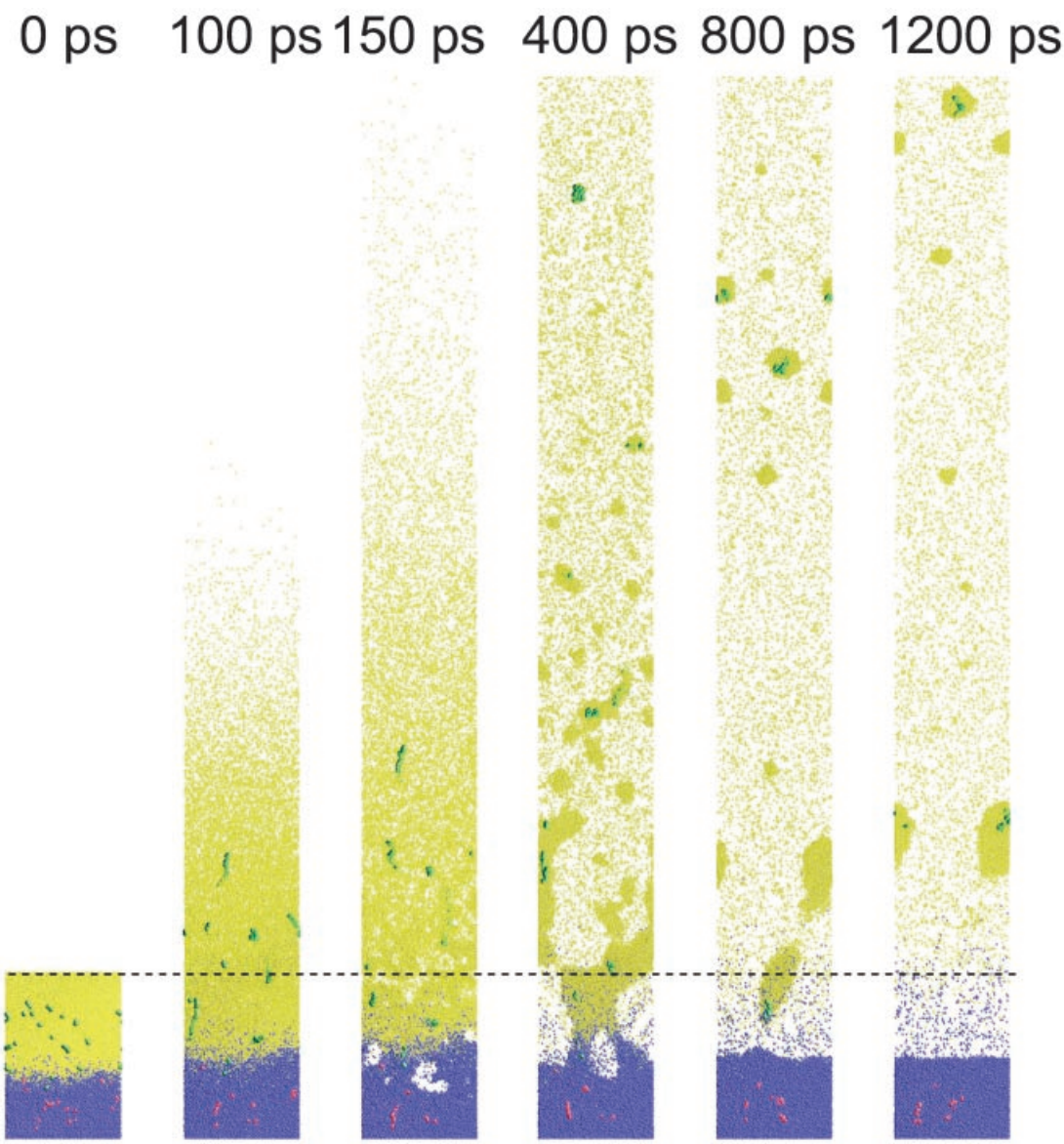

FIGURE 18. Time snapshots for a MALDI simulation. The matrix and analyte molecules that ablate are yellow and green, respectively. The matrix and analyte molecules that do not ablate are blue and red. Only molecules in a slice 3 nm thick are shown. The horizontal dimension of each snapshot is 40 nm and the vertical dimension is 380 nm. The dashed line is the position of the original surface. The data are from Leveugle and Zhigilei (2007). *Animation 8*.

of modeling of ionization in organic-like solids. First, Knochenmuss proposed an energy pooling mechanism for ion formation in MALDI (Knochenmuss, 2002). His studies include ground and excited state matrix and analyte species, and ions. He showed that there is a competition in the plume among the matrix and analyte molecules for the ions which leads to an explanation of matrix and analyte suppression effects (Knochenmuss, 2003). Recently, Knochenmuss and Zhigilei (2005) have incorporated the energy pooling mechanism into a MD simulation of laser ablation. They find that free matrix ions are formed in both the desorption and ablation regime although as discussed above, they find that the analyte ions remain embedded in clusters composed of matrix molecules throughout the simulation time (several nanosecond). In the second study, Wojciechowski and co-workers examined the emission of pre-formed salt ions from a water matrix in SIMS in a joint computation and experimental study (Wojciechowski et al., 2004a,b) They found experimentally that for over four orders of magnitude of salt concentration the ion intensities are relatively constant and more cations are emitted than anions. Moreover, for 1 M solutions the bare ion (e.g., Na^+ or I^-) is the predominant species over hydrated ions. The simulations demonstrate that at high concentration of salt the cations and anions neutralize each other, thus inhibiting ejection as ions. At the highest concentrations, there are local areas in the water

where there are nearby pairs of ions of like charge that repel each other in the desorption event and thus eject as bare ions. Due to limited ionization processes included and the limited size of the simulation, the modeling could not explain the hydrated ion, for example, $Na^+(H_2O)_n$, distributions, differences in the spectra among different salt compounds and the experimentally observed distributions of $(H_2O)_n^+$, $(H_2O)_nH^+$, and $(H_2O)_nOH^-$.

There is an essential difference in these two simulations relative to the number of particles in the simulation versus the number of ions ejected. In the MALDI simulations, approximately 10^6 particles eject. For an ion fraction of 10^{-5} to 10^{-3} (Dreisewerd, 2003) a total of 10 to 1,000 ions are ejected in one simulation. In SIMS the ion fractions are similar, but only on the order of 10^3 or fewer particles eject per incident particle which means that one simulation may give no ions at all. Thus, hundreds of trajectories, each of weeks to months (Table I), would have to be performed in order to make comparisons with experimental distributions.

Thus, although steps have been initiated at understanding ionization in MALDI and SIMS, there is enormous room for improvement. The studies described above assume a specific mechanism of ion formation, energy pooling of molecules in excited electronic states or pre-formed ions, and then examine the consequences of the assumed mechanism on some property that can be measured in experiment. Ideally it would be nice to have a first principles calculation of ionization and electronic effects. At this time, however, we do not know of a formalism to include all possible processes. It is evident, however, that it must involve quantum mechanics. Quantum mechanical calculations are simply too big to perform for systems of the size needed for SIMS and MALDI. Thus, for the time being, the only tractable approach is to develop models with assumed ionization processes and test them against experimental data.

To illustrate the intricacies of modeling ionization and verifying the reasonableness of the results, consider the possibility of modeling the $(M + H)^+$ ion intensity in cluster SIMS of a system of a biological molecule, M, in ice, a natural biological matrix. Certainly, there might be preformed ions, $(M + H)^+$, but there is also a plume-like evolution (Wojciechowski & Garrison, 2006) which can lead to a competition for the charged particle by the various species in the system as in the Knochenmuss MALDI simulations. Simulations of cluster bombardment of water ice show that there is ample energy to dissociate water molecules during the bombardment event (Ryan et al., 2007). Thus, the creation of new ions and attachment of the new ions to the molecule is possible. Moreover, the same simulations (Ryan et al., 2007) as well as the study of pre-formed ions by Wojciechowski et al. (2004a,b) show that recombination of near-by ions to form neutral species is very probable. In addition to the formation of parent $(M + H)^+$ ions the model should, therefore, predict all the water cluster distributions mentioned above.

Concomitant with the computational complexities is whether experimental data is sufficiently discriminating to determine if the assumed ionization mechanism is correct or not. For example, for cluster SIMS studies of ice, it has been shown that the water cluster distributions, $(H_2O)_nH^+$, have differences that are characteristic of the projectile, C_{60}^+, Au_3^+ or Au^+ (Conlan et al., 2006a). Other studies give that ion yields, $(M + H)^+$, of small peptides in ice depend on the basicity of the peptide (Conlan, Lockyer, & Vickerman, 2006). At the same time the estimate for the total ion yield is $\sim 10^{-2}$ (Szakal, Kozole, & Winograd, unpublished work). At this stage it is impossible to tell if these data would allow one to make a definitive statement about mechanisms. The challenge to understand ionization, especially in SIMS, requires not only good theory and modeling but also experimental data that will discriminate among various possible ionization mechanisms that might be assumed in a theory or model. Therefore, the challenge to both theorists and experimentalists is to design appropriate models and experiments.

IX. CONCLUSION

The molecular dynamics simulations provide a unique view into the basic processes in surface based mass spectrometries. The overarching concept from the simulations that underpins the success of all the techniques to launch non-volatile molecules into the gas phase for analysis is some level of correlation or cooperativity of motion. It is the cooperative motion that propels the molecules off the surface without attaining thermal equilibrium with the internal vibrational modes that would lead to dissociation or rearrangement. For atomic SIMS, this cooperative motion is occasional, much like a game of billiards. For cluster SIMS, the atoms in the cluster strike the surface creating a crater, thus there is a consistency of correlated motion from one impact to the next. Increasing the cluster size even further introduces a washing mechanism to remove molecules from the surface, again with a large level of correlated motion although much of motion is in the horizontal direction. The technique that masters correlated motion towards the vacuum and detector is MALDI. In this technique, there is a phase transition or explosive boiling that drives a billion times more mass into the vacuum than is possible with cluster beams.

The basic physics provides only one piece of the consideration in choosing one surface based mass spectrometry over another. There are many experimental considerations. If the sample needs to be neat (i.e., no matrix), then particles rather than a laser are the energizer of choice. Atomic and cluster SIMS provide for the highest resolution imaging capability. Cluster beams such as C_{60} allow for molecular depth profiling. DESI with the massive liquid droplets can be performed in atmospheric conditions opening the door for many unique applications. Finally, there is the issue of ionization which is still unknown and may be the deciding factor for one technique to give the best signal for a given system.

ACKNOWLEDGMENTS

The financial support from the National Science Foundation grant # CHE-0456514 and the Polish Ministry of Science and Higher Education programs no. PB 4097/H03/2007/33 and PB2030/H03/2006/31 are gratefully acknowledged. The Academic Services and Emerging Technologies group at Penn State provided us early access to the lion-xo PC cluster. Leonid Zhigilei and Elodie Leveugle provided the data for Figure 18. Finally, we would like to thank our current and former

collaborators who have contributed to our understanding of surface based mass spectrometry and our enjoyment of performing simulations to match with experiment. Mike Russo, Kate Ryan and two excellent reviewers critically read the manuscript.

REFERENCES

Aderjan R, Urbassek HM. 2000. Molecular-dynamics study of craters formed by energetic Cu cluster impact on Cu. Nucl Instrum Methods Phys Res Sect B 164:697–704.

Allen MP, Tildesley DJ. 1987. Computer simulation of liquids. Oxford: Clarendon Press.

Anders C, Urbassek HM. 2005a. Cluster-size dependence of ranges of 100 eV/atom Au_n clusters. Nucl Instrum Methods Phys Res Sect B 228:57–63.

Anders C, Urbassek HM. 2005b. Effects of binding energy and mass in cluster-induced sputtering of van-der-Waals bonded systems. Nucl Instrum Methods Phys Res Sect B 228:84–91.

Anders C, Kirihata H, Yamaguchi Y, Urbassek HM. 2007. Ranges and fragmentation behavior of fullerene molecules: A molecular-dynamics study of the dependence on impact energy and target material. Nucl Instrum Methods Phys Res Sect B 255:247–252.

Aoki T, Matsuo J. 2006. Molecular dynamics simulations of surface modification and damage formation by gas cluster ion impacts. Nucl Instrum Methods Phys Res Sect B 242:517–519.

Aoki T, Seki T, Matsuo J, Insepov Z, Yamada I. 1998. Molecular dynamics simulation of a carbon cluster ion impacting on a carbon surface. Mater Chem Phys 54:139–142.

Aoki T, Chiba S, Matsuo J, Yamada I, Biersack JP. 2001. Molecular dynamics and Monte-Carlo simulation of sputtering and mixing by ion irradiation. Nucl Instrum Methods Phys Res Sect B 180:312–316.

Aoki T, Matsuo J, Takaoka G, Yamada I. 2003. Cluster species and cluster size dependence of damage formation by cluster ion impact. Nucl Instrum Methods Phys Res Sect B 206:861–865.

Asakawa D, Fujimaki S, Hashimoto Y, Mori K, Hiraoka K. 2007. Study on ion formation in electrospray droplet impact secondary ion mass spectrometry. Rapid Commun Mass Spectrom 21:1579–1586.

Atkins P, dePaula J. 2006. Physical Chemistry.

Bolbach G, Beavis R, Dellanegra S, Deprun C, Ens W, Lebeyec Y, Main DE, Schueler B, Standing KG. 1988. Variation of yield with thickness in Sims and Pdms—Measurements of secondary ion emission from organized molecular films. Nucl Instrum Methods Phys Res Sect B 30:74–82.

Brenner DW. 1990. Empirical potential for hydrocarbons for use in simulating the chemical vapor-deposition of diamond films. Phys Rev B 42:9458–9471.

Brenner DW, Shenderova OA, Harrison JA, Stuart SJ, Ni B, Sinnott SB. 2002. A second-generation reactive empirical bond order (REBO) potential energy expression for hydrocarbons. J Phys Condens Mat 14:783–802.

Chatterjee R, Postawa Z, Winograd N, Garrison BJ. 1999. Molecular dynamics simulation study of molecular ejection mechanisms: keV particle bombardment of C_6H_6/Ag{111}. J Phys Chem B 103:151–163.

Cheng J, Wucher A, Winograd N. 2006. Molecular depth profiling with cluster ion beams. J Phys Chem B 110:8329–8336.

Cheng J, Kozole J, Hengstebeck R, Winograd N. 2007. Direct comparison of Au-3(+) and C-60(+) cluster projectiles in SIMS molecular depth profiling. J Am Soc Mass Spectrom 18:406–412.

Colla TJ, Urbassek HM. 2000. Au sputtering by cluster bombardment: A molecular dynamics study. Nucl Instrum Methods Phys Res Sect B 164:687–696.

Colla TJ, Aderjan R, Kissel R, Urbassek HM. 2000. Sputtering of Au (111) induced by 16-keV Au cluster bombardment: Spikes, craters, late emission and fluctuations. Phys Rev B 62:8487–8493.

Conlan XA, Biddulph GX, Lockyer NP, Vickerman JC. 2006a. Using polyatomic primary ions to probe an amino acid and a nucleic base in water ice. Appl Surf Sci 252:6506–6508.

Conlan XA, Lockyer NP, Vickerman JC. 2006b. Is proton cationization promoted by polyatomic primary ion bombardment during time-of-flight secondary ion mass spectrometry analysis of frozen aqueous solutions? Rapid Commun Mass Spectrom 20:1327–1334.

Cooks RG, Ouyang Z, Takats Z, Wiseman JM. 2006. Ambient mass spectrometry. Science 311:1566–1570.

Cornett DS, Lee TD, Mahoney JF. 1994. Matrix-free desorption of biomolecules using massive cluster-impact. Rapid Commun Mass Spectrom 8:996–1000.

Czerwinski B, Delcorte A, Garrison B, Samson R, Winograd N, Postawa Z. 2006. Sputtering of thin benzene and polystyrene overlayers by keV Ga and C-60 bombardment. Appl Surf Sci 252:6419–6422.

Czerwinski B, Rzeznik L, Stachura K, Paruch R, Garrison BJ, Postawa Z. 2008. Applications of fullerene beams in analysis of thin layers. Vacuum (in press).

Delcorte A, Garrison BJ. 2000. High yield events of molecular emission induced by kiloelectronvolt particle bombardment. J Phys Chem B 104:6785–6800.

Delcorte A, Garrison BJ. 2007. Sputtering polymers with buckminsterfullerene projectiles: A coarse-grained molecular dynamics study. J Phys Chem C 111:15312–15324.

Dou YS, Winograd N, Garrison BJ, Zhigilei LV. 2003. Substrate-assisted laser-initiated ejection of proteins embedded in water films. J Phys Chem B 107:2362–2365.

Dreisewerd K. 2003. The desorption process in MALDI. Chem Rev 103:395–425.

Dreisewerd K, Schurenberg M, Karas M, Hillenkamp F. 1995. Influence of the laser intensity and spot size on the desorption of molecules and ions in matrix-assisted laser-desorption ionization with a uniform beam profile. Int J Mass Spectrome Ion Processes 141:127–148.

Fletcher JS, Lockyer NP, Vaidyanathan S, Vickerman JC. 2007. TOF-SIMS 3D biomolecular imaging of Xenopus laevis oocytes using buckminsterfullerene (C-60) primary ions. Anal Chem 79:2199–2206.

Foiles SM, Baskes MI, Daw MS. 1986. Embedded-atom-method functions for the Fcc metals Cu, Ag, Au, Ni, Pd, Pt, and their alloys. Phys Rev B 33:7983–7991.

Frenkel D, Smit B. 2002. Understanding molecular simulation from algorithms to applications. Sandiego: Academic Press.

Garrison BJ. 1980. Mechanisms of ejection of organic molecules from surfaces by keV ion bombardment. J Am Chem Soc 102:6553–6555.

Garrison BJ. 1992. Molecular-dynamics simulations of surface chemical-reactions. Chem Soci Rev 21:155–162.

Garrison BJ. 2001. Molecular dynamics simulations, the theoretical partner to static SIMS experiments. In: Vickerman JC, Briggs D, editors. ToF-SIMS: Surface analysis by mass spectrometry. Manchester: Surface Spectra. pp. 223–257.

Garrison BJ, Srivastava D. 1995. Potential-energy surfaces for chemical-reactions at solid-surfaces. Annu Rev Phys Chem 46:373–394.

Garrison BJ, Delcorte A, Krantzman KD. 2000. Molecule liftoff from surfaces. Acc Chem Res 33:69–77.

Garrison BJ, Kodali PBS, Srivastava D. 1996. Modeling of surface processes as exemplified by hydrocarbon reactions. Chem Rev 96:1327–1341.

Garrison BJ, Itina TE, Zhigilei LV. 2003. Limit of overheating and the threshold behavior in laser ablation. Phys Rev E 68:041501.

Garrison BJ, Ryan KE, Russo MF, Smiley EJ, Postawa Z. 2007. Quadratic friction model for cluster bombardment of molecular solids. J Phys Chem C 111:10135–10137.

Handschuh M, Nettesheim S, Zenobi R. 1999. Laser-induced molecular desorption and particle ejection from organic films. Appl Surf Sci 137:125–135.

Hillenkamp F, Karas M, Beavis RC, Chait BT. 1991. Matrix-assisted laser desorption ionization mass-spectrometry of biopolymers. Anal Chem 63:A1193–A1202.

Hiraoka K, Asakawa D, Fujimaki S, Takamizawa A, Mori K. 2006a. Electrosprayed droplet impact/secondary ion mass spectrometry. Eur Phys J D 38:225–229.

Hiraoka K, Mori K, Asakawa D. 2006b. Fundamental aspects of electrospray droplet impact/SIMS. J Mass Spectrom 41:894–902.

Itina TE, Zhigilei LV, Garrison BJ. 2002. Microscopic mechanisms of matrix assisted laser desorption of analyte molecules: Insights from molecular dynamics simulation. J Phys Chem B 106:303–310.

Johnson RE. 1996. Models for Matrix Assisted Laser Desorption and Ionization: MALDI. In: Baer T, Ng CY, Powis I, editors. Large ions: Their vaporization, detection and structural analysis. New York: John Wiley. p. 49.

Kelchner CL, Halstead DM, Perkins LS, Wallace NM, Depristo AE. 1994. Construction and evaluation of embedding functions. Surf Sci 310: 425–435.

Kerford M, Webb RP. 2001. Desorption of molecules by cluster impact. A preliminary molecular dynamics study. Nucl Instrum Methods Phys Res Sect B 180:44–52.

Knochenmuss R. 2002. A quantitative model of ultraviolet matrix-assisted laser desorption/ionization. J Mass Spectrom 37:867–877.

Knochenmuss R. 2003. A quantitative model of ultraviolet matrix-assisted laser desorption/ionization including analyte ion generation. Anal Chem 75:2199–2207.

Knochenmuss R, Zhigilei LV. 2005. Molecular dynamics model of ultraviolet matrix-assisted laser desorption/ionization including ionization processes. J Phys Chem B 109:22947–22957.

Kristyan S, Bencsura A, Vertes A. 2002. Modeling the cluster formation during infrared and ultraviolet matrix-assisted laser desorption ionization of oligonucleotides in succinic acid matrix with molecular mechanics. Theor Chem Acc 107:319–325.

Leveugle E, Zhigilei LV. 2007. Molecular dynamics simulation study of the ejection and transport of polymer molecules in Matrix-Assisted Pulsed Laser Evaporation (MAPLE). J Appl Phys 102:074914.

Li Z, Verkhoturov SV, Schweikert EA. 2006. Nanovolume analysis with secondary ion mass spectrometry using massive projectiles. Anal Chem 78:7410–7416.

Mahoney JF, Perel J, Lee TD, Martino PA, Williams P. 1992. Shock-wave model for sputtering biomolecules using massive cluster impacts. J Am Soc Mass Spectrom 3:311–317.

McDonnell LA, Heeren RMA. 2007. Imaging mass spectrometry. Mass Spectrom Rev 26:606–643.

Postawa Z, Czerwinski B, Szewczyk M, Smiley EJ, Winograd N, Garrison BJ. 2003. Enhancement of sputtering yields due to C_{60} versus Ga bombardment of Ag{111} as explored by molecular dynamics simulations. Anal Chem 75:4402–4407.

Postawa Z, Czerwinski B, Szewczyk M, Smiley EJ, Winograd N, Garrison BJ. 2004. Microscopic insights into the sputtering of Ag{111} induced by C_{60} and Ga bombardment. J Phys Chem B 108:7831–7838.

Postawa Z, Czerwinski B, Winograd N, Garrison BJ. 2005. Microscopic insights into the sputtering of thin organic films on Ag{111} induced by C_{60} and Ga bombardment. J Phys Chem B 109:11973–11979.

Prasad M, Conforti PF, Garrison BJ. 2007. Coupled molecular dynamics—Monte Carlo model to study the role of chemical processes during laser ablation of polymeric materials. J Chem Phys 127:084705.

Russo MF Jr, Garrison BJ. 2006. Mesoscale energy deposition footprint model for keV cluster bombardment of solids. Anal Chem 78:7206–7210.

Russo MF Jr, Wojciechowski IA, Garrison BJ. 2006. Sputtering of amorphous ice induced by C_{60} and Au_3 clusters. Appl Surf Sci 252:6423–6425.

Russo MF Jr, Szakal C, Kozole J, Winograd N, Garrison BJ. 2007. Sputtering yields for C_{60} and Au_3 bombardment of water ice as a function of incident kinetic energy. Anal Chem 79:4493–4498.

Ryan KE, Wojciechowski IA, Garrison BJ. 2007. Reaction dynamics following keV cluster bombardment. J Phys Chem C 111:12822–12826.

Ryan KE, Smiley EJ, Winograd N, Garrison BJ. 2008. Angle of incidence effects in a molecular solid. Appl Surf Sci (in press).

Rzeznik L, Czerwinski B, Garrison BJ, Winograd N, Postawa Z. 2008. Microscopic insights into the sputtering of thin polystyrene films on Ag{111} induced by large and slow Ar clusters. J Phys Chem C 112(2): 521–531.

Sadeghi M, Wu XW, Vertes A. 2001. Conformation changes, complexation, and phase transition in matrix-assisted laser desorption. J Phys Chem B 105:2578–2587.

Seki T, Aoki T, Tanomura M, Matsuo J, Yamada I. 1998. Energy dependence of a single trace created by C_{60} ion impact. Mater Chem Phys Lipids 54:143–146.

Seki T, Murase T, Matsuo J. 2006. Cluster size dependence of sputtering yield by cluster ion beam irradiation. Nucl Instrum Methods Phys Res Sect B 242:179–181.

Smiley EJ, Postawa Z, Wojciechowski IA, Winograd N, Garrison BJ. 2006. Coarse-grained molecular dynamics studies of cluster-bombarded benzene crystals. Appl Surf Sci 252:6436–6439.

Smiley EJ, Winograd N, Garrison BJ. 2007. Effect of cluster size in kiloelectronvolt cluster bombardment of solid benzene. Anal Chem 79:494–499.

Sostarecz AG, Sun S, Szakal C, Wucher A, Winograd N. 2004. Depth profiling studies of multilayer films with a C_{60}^+ ion source. Appl Surf Sci 231–2:179–182.

Srinivasan R, Braren B. 1989. Ultraviolet-laser ablation of organic polymers. Chem Rev 89:1303–1316.

Stillinger FH, Weber TA. 1985. Computer-simulation of local order in condensed phases of silicon. Phys Rev B 31:5262–5271.

Stuart SJ, Tutein AB, Harrison JA. 2000. A reactive potential for hydrocarbons with intermolecular interactions. J Chem Phys 112: 6472–6486.

Szakal C, Kozole J, Russo MF Jr, Garrison BJ, Winograd N. 2006. Surface sensitivity in cluster-ion-induced sputtering. Phys Rev Lett 96:216104.

Takats Z, Wiseman JM, Gologan B, Cooks RG. 2004. Mass spectrometry sampling under ambient conditions with desorption electrospray ionization. Science 306:471–473.

Takats Z, Wiseman JM, Cooks RG. 2005. Ambient mass spectrometry using desorption electrospray ionization (DESI): Instrumentation, mechanisms and applications in forensics, chemistry, and biology. J Mass Spectrom 40:1261–1275.

Tempez A, Schultz JA, Della-Negra S, Depauw J, Jacquet D, Novikov A, Lebeyec Y, Pautrat M, Caroff M, Ugarov M, Bensaoula H, Gonin M, Fuhrer K, Woods A. 2004. Orthogonal time-of-flight secondary ion mass spectrometric analysis of peptides using large gold clusters as primary ions. Rapid Commun Mass Spectrom 18:371–376.

Tersoff J. 1988. Empirical interatomic potential for silicon with improved elastic properties. Phys Rev B 38:9902–9905.

Tersoff J. 1989. Modeling solid-state chemistry: Interatomic potentials for multicomponent systems. Phys Rev B 39:5566–5568.

Webb R, Kerford M, Way A, Wilson I. 1999. Comparison of gold and carbon cluster impacts on graphite using Molecular Dynamics simulation. Nucl Instrum Methods Phys Res Sect B 153:284–291.

Weibel D, Wong S, Lockyer N, Blenkinsopp P, Hill R, Vickerman JC. 2003. A C_{60} primary ion beam system for time of flight secondary ion mass spectrometry: Its development and secondary ion yield characteristics. Anal Chem 75:1754–1764.

Winograd N. 2005. The magic of cluster SIMS. Anal Chem 77:142A–149A.

Wojciechowski IA, Garrison BJ. 2006. Sputtering of water ice induced by C_{60} bombardment: Onset of plume formation. J Phys Chem A 110:1389–1392.

Wojciechowski I, Sun JM, Szakal C, Winograd N, Garrison BJ. 2004a. Ion emission from water ice due to energetic particle bombardment. J Phys Chem A 108:2993–2998.

Wojciechowski IA, Kutliev U, Sun SX, Szakal C, Winograd N, Garrison BJ. 2004b. Emission of ionic water clusters from water ice films bombarded by energetic projectiles. Appl Surf Sci 231–2:72–77.

Wong SCC, Lockyer NP, Vickerman JC. 2005. Mechanisms of secondary ion emission from self-assembled monolayers and multilayers. Surf Interface Anal 37:721–730.

Wucher A, Garrison BJ. 1992. Unimolecular decomposition in the sputtering of metal-clusters. Phys Rev B 46:4855–4864.

Wucher A, Cheng J, Winograd N. 2007. Protocols for three-dimensional molecular imaging using mass spectrometry. Anal Chem 79:5529–5539.

Yamada I, Matsuo J, Toyoda N, Ion CRCC. 2003. Cluster ion beam process technology. Nucl Instrum Methods Phys Res Sect B 206:820–829.

Yingling YG, Zhigilei LV, Garrison BJ, Koubenakis A, Labrakis J, Georgiou S. 2001. Laser ablation of bicomponent systems: A probe of molecular ejection mechanisms. Appl Phys Lett 78:1631–1633.

Yingling YG, Conforti PF, Garrison BJ. 2004. Theoretical investigation of laser pulse width dependence in the thermal confinement regime. Appl Phys A 79:757–759.

Zhigilei LV, Garrison BJ. 1998. Velocity distributions of analyte molecules in matrix-assisted laser desorption from computer simulations. Rapid Commun Mass Spectrom 12:1273–1277.

Zhigilei LV, Garrison BJ. 1999a. Molecular dynamics simulation study of the fluence dependence of particle yield and plume composition in laser desorption and ablation of organic solids. Appl Phys Lett 74:1341–1343.

Zhigilei LV, Garrison BJ. 1999b. Pressure waves in microscopic simulations of laser ablation. Mater Res Soc Symp Proc 538:491–496.

Zhigilei LV, Garrison BJ. 2000. Microscopic mechanisms of laser ablation of organic solids in the thermal and stress confinement irradiation regimes. J Appl Phys 88:1281–1298.

Ziegler JF, Biersack JP, Littmark U. 1985. The stopping and range of ions in solids. New York: Permagon Press.

Zhigilei LV, Kodali PBS, Garrison BJ. 1997. Molecular dynamics model for laser ablation and desorption of organic solids. J Phys Chem B 101: 2028–2037.

Zhigilei LV, Kodali PBS, Garrison BJ. 1998. A microscopic view of laser ablation. J Phys Chem B 102:2845–2853.

Zhigilei LV, Leveugle E, Garrison BJ, Yingling YG, Zeifman MI. 2003a. Computer simulations of laser ablation of molecular substrates. Chem Rev 103:321–347.

Zhigilei LV, Yingling YG, Itina TE, Schoolcraft TA, Garrison BJ. 2003b. Molecular dynamics simulations of matrix-assisted laser desorption—Connections to experiment. Int J Mass Spectrom 226:85–106.

Barbara J. Garrison received her Ph.D. in 1975 at the University of California at Berkeley, where her mentors were Professors William A. Lester, Jr., William H. Miller and Henry F. Schaefer, III. After a postdoctoral appointment at Purdue University, she joined the chemistry faculty of Penn State University in 1979. Her group is actively involved in understanding fast energy deposition processes at surfaces.

Zbigniew Postawa received his Ph.D. in 1987 at the Jagiellonian University in Krakow, Poland, where his mentor was Professor Marek Szymonski. After a postdoctoral appointment at the Pennsylvania State University, he joined the physics faculty of the Jagiellonian University in 1991. His group is involved in understanding of processes stimulated in solid surfaces by impact of monoatomic and cluster projectiles.